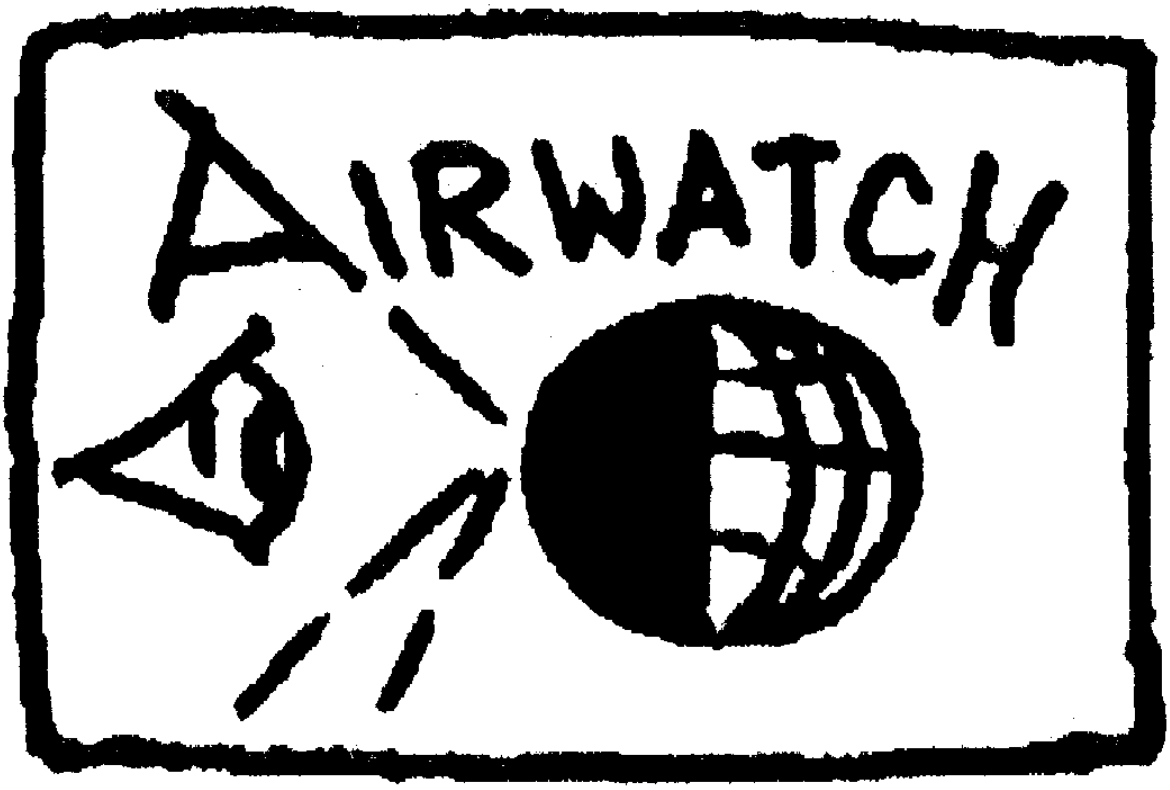

“AIRWATCH FROM SPACE”
Progress report
By

Osvaldo Catalano

IFCAI – CNR, Palermo

Introduction

This report presents the results of a preliminary study as a part of the "AIRWATCH FROM SPACE" project. The motivation for this work is to:

- Qualify and characterize the proposed **FIRE** (Fluorescence Image Readout Electronics), as suitable for such an experiment.
- Study the performance of the system introducing the physics context by means of computation and Montecarlo simulation.

The idea of AIRWATCH FROM SPACE is based on the property that charged particles interacting with air molecules produce light in the UV range. This property has been used successfully for ground observation of EAS (Extensive Air Showers) by previous experiments such as Fly's Eye[1]. The limitation of ground observation of the fluorescence light is severe if the energy of the particle producing the shower is of the order of 10^{20} eV. In that case the frequency of such events is so small that to succeed to observe, in average, one event per year, 1000 Km^2 of territory has to be monitored (assuming the duty cycle of 10%). The goal of AIRWATCH FROM SPACE is to extend, as much as possible the target area making use of a satellite equipped with a wide-angle optics looking down toward the Earth from a distance of order of 500 Km.. Figure 1 shows an artistic view of the satellite-Earth system. Larger target area implies, naturally, a larger active detection area and consequently a larger number of UV sensor elements.

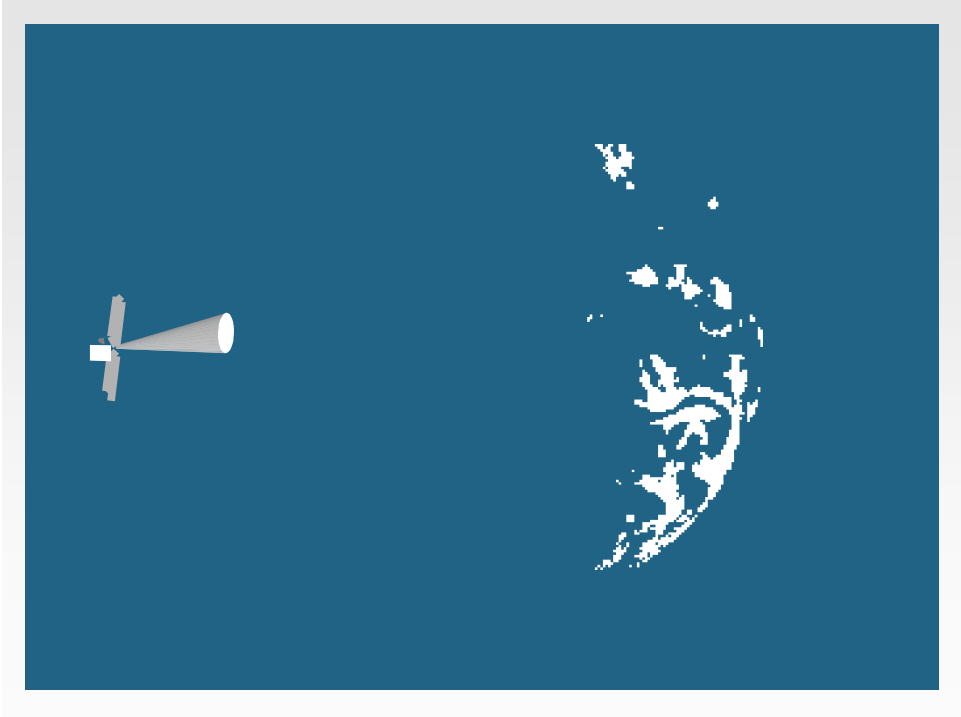

Fig. 1. Artistic view of satellite-Earth system.

The demanding requirements imposed by the project: the very high pixelization together with the detection of faint signals, have been the starting point for considering an approach based on a technique making use of single photon counting with fast detectors and electronics (≈ 10 ns resolving time). This suggests using digitized signals which make it possible to design a read-out electronics much simpler and less expensive than the analog type. Additional advantages of the present digital electronic components are low power consumption, small space requirement and low cost. This matches the requirements of a satellite enterprise.

- A description of key-words and definitions used in the report is given in the first section.
- A description of the front end, read-out electronics and trigger is presented in some detail in the second section of this report.
- A description of the simulation of the FIRE system together with simulated physical phenomena is contained in the third section of the report.
- The fourth section shows preliminary results obtained using Montecarlo simulation. Also shown are sample printouts extracted from the event display program written by the author.
- The fifth section introduces the potentiality of “Airwatch from Space” in detecting neutrino events.
- Future plans and concluding remarks close the report.

As this is a description of an entire project which is far from completeness in each of its parts, some assumptions have been made for the purpose of designing the “FIRE” system and simulating its performance. The assumptions that are made are declared step by step, whenever it is necessary.

1. Key-words and global definitions

The Goal is an IMAGE of an EVENT (These ideas are implicit in "watch")

The general goal of AIRWATCH, applied to EECR (Extreme Energy Cosmic Ray), is to acquire images of events that occur when an individual EECR -- a nucleus, a gamma ray or a neutrino -- strikes the air. When EECR encounter the atmosphere they produce UV photons as an end result of a complex relativistic cascade process whose over-all manifestation has the name 'Extensive Air Shower' (EAS).

TRACK/TRACE

Viewed at some instant from a distance, an EAS appears as a relatively small disk-shaped luminous object. When it is viewed continuously, the object moves on a straight path with the speed of light. As it does so, the luminosity changes continuously from being so faint it is undetectable, up to a maximum. Then it gradually fades. At the time it reaches sea level, the transverse dimension of the disk (track width) is roughly (of the order) 100 m; the thickness of the disk is roughly 10 m. The distance traveled during the 'bright phase' (track length) is roughly 10 Km. All of the dimensions as width, thickness and length, depend somewhat on the air density. Tracks of vertical EECR come to an end where the EAS encounters the earth's surface. (It is possible, in case of nearly horizontal tracks, for a track to simply fade away, and for the EAS to leave the atmosphere, due to the earth's curvature, but this type of track is so unusual that it will be neglected here).

REAL OBJECT SPACE (ROS)

The ROS is described by continuous (analog) variables. It is curved to fit the real Earth. The boundary with the earth's solid surface may have various properties. There may or may not be clouds. In this space the FOV (Field Of View) is the interior of a cone made up of light rays. The axis of the cone may or may not have exactly the nominal value. The intersection of the cone with the earth's surface is approximately a circle. The air contained in the ROS may have various temperature and density profiles.

VIRTUAL OBJECT SPACE (VOS)

The VOS is bounded by the frustum of a square pyramid whose base plane is horizontal, tangent to a point on the earth's surface directly beneath the apex of the pyramid (at the satellite), and whose top plane is horizontal at a height Z taken as the 'top of the atmosphere'. The base of the VOS corresponds in some average sense to the approximately circular intersection of the ROS referred to above.

The VOS is composed of horizontal layers with equal thickness ct, where c is the velocity of light and t is an important parameter of the FIRE system, named CRT (Cell Resolving Time). The layers are numbered 1,2,3,…NN, downward, starting at the top plane. Thus NN=Z/ct. The base of the VOS is divided in N*N

equal squares, each of which is the base of a pyramid with the same apex as the VOS. The set of squares formed by the intersection of an ‘elemental pyramid’ and the successive horizontal layers. In the VOS context, the term ‘pixel’ denotes any of the small squares produced in this way. The specification of a particular VOS pixel requires 3 whole numbers belonging to X, Y and Z.

IMAGE SPACE (IS)

The FIRE image space is digitized and has analogous structure to the VOS. As the word ‘image’ implies, there is a one-one reciprocal correspondence between cells of the VOS and IS, as defined by the FIRE system. The image space is symbolic, without dimensions, described only by sets of whole numbers that specify X, Y and Z. Initially the question is left open about the phase relation between the layer numbers (indices) in the VOS and the corresponding numbers used by the FIRE system. The architecture of the FIRE system has intermediate levels of organization, both for the X, Y planes and for time. Time corresponds to the Z dimension of VOS. In the FIRE system, the pixels are organized in K*K equal ‘macrocell’, each consisting of n*n pixels (thus N=k*n. The whole numbers k and n are important parameters of FIRE). The CRT, numbered sequentially with respect to some ‘trigger time’ specified below are grouped in terms of ‘Gate Time Unit’ (GTU) whose duration, in terms of CRT, is another important FIRE parameter. The value used in the FIRE report is about 83 (CRT=10 ns).

The following section (Section 2) spells out in detail how the FIRE system deals with Image Space.

In section 3 and 4, virtual EAS events are generated in VOS by Montecarlo simulations, and it is shown with examples how simulated input data are used by the FIRE system to perform the functions of triggering and digital recording.

2.The “FIRE” system

The idea of a modular structure is at the base of the FIRE system. The capability of reading as few channels as possible without losing information is very important in the economy of the project. Moreover modularity is ideal for satellite experiments. Modularity has been preferred to satisfy the requirements of flexibility, easy planning and implementation, and redundancy. Reduction in total number of read-out channels is also one of the primary objectives in the design of the electronics, and it has been accomplished using a simple design that manages the connections with adjacent pixels (respectively by rows and by columns) OR-ing them together.
In the assumption of a fast detector with a CRT of the order of 10 ns, capable of counting the single photoelectrons, the proposed read-out electronics is able to register position and arrival time (x_i, y_i, t_i) of detected photoelectrons by combining the two projections X and Y, to give the position, and then recording separately the relative arrival times of the individual photoelectrons.
We use the ’free running’ method, based on continuously writing into memories until a stop signal, derived from a specialized trigger unit, freezes the writing operation. At the stop signal a reading operation is started that enables accessing the information recorded in the memories, both for position and time. The digitized information is now ready to be transmitted in telemetry to the ground station at a very low baud rate.

2.1 Focal Plane Layout

The “detector” at the focal plane is our name for the functional equivalent of an eye’s retina. It is foreseen as having an intermediate stage of organization being organized as a bi-dimensional array of macrocells. Each of the of K*K macrocells is a bi-dimensional array of n*n pixels. The pixels of the detector act like the individual cells of a retina.
The use of the term “macrocell” is referred at one module whereas “pixel” is the basic unit constituting with many others a macrocell. The macrocells form the detection area at the focal plane. Figure 2 shows the focal plane organized in macrocells and the macrocell organized in pixels.

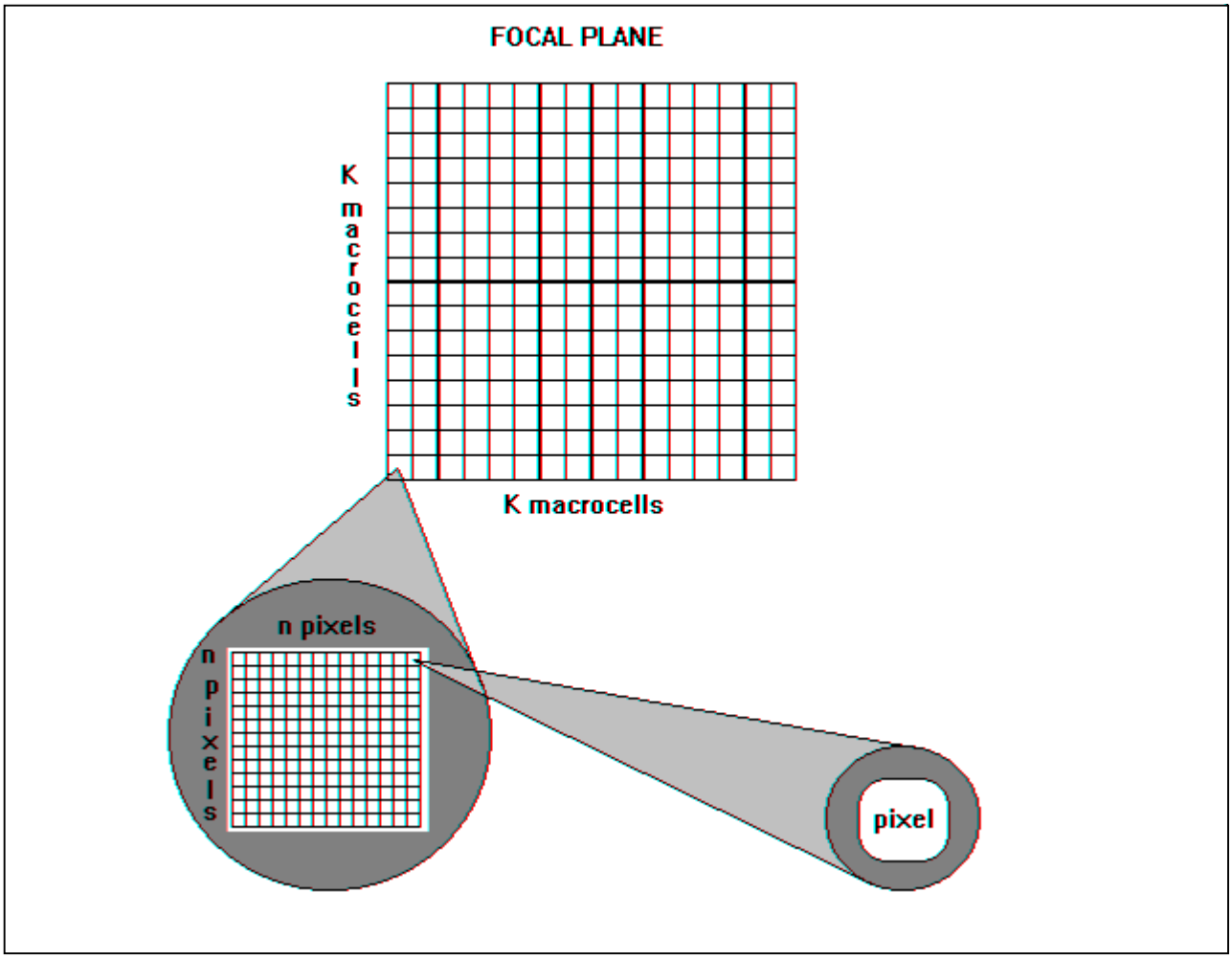

Fig. 2. Schematic view of the focal plane and macrocell layout.

This configuration permits us to treat each macrocell as a detection unit independent of the other macrocells, thus simplifying the design of our front-end electronics, making it consist simply of a repetition of the same unit. Moreover, the organization of the focal plane in macrocells offers the advantages of redundancy, easy maintenance in the test and calibration phase, light weight mechanical structure and so on.

2.2 Individual Pixel Detector Front-End

The function of a pixel front-end is to:

- transform the analogue detector signal into a digital signal (with a fast single threshold discriminator);
- count the digitized pulses and enable the output at a programmable digital threshold (with a programmable resetable counter);
- split the signals for the X and Y positions (using open-collector buffers) and for the timing channel (using an open-collector AND gate).

Figure 3 shows schematically the pixel front-end electronics. The main goal of this front-end is to reduce the pixel background rate by enhancing the signal to noise property. This is realized by setting the "set count" input of the programmable counter at an integer value **m,** corresponding to the Poissonian probability P_m to find in one pixel at least **m** photoelectrons in one GTU. The signal to background ratio becomes $\mathbf{(S-m+1)/\sqrt{P_m}}$, where **S** is the total number of photoelectrons in a pixel per GTU.
The simplicity of the pixel front-end electronics permits us to build it, possibly, in ASIC (Application Specific Integrated Circuits) device, allowing for a large-scale integration.

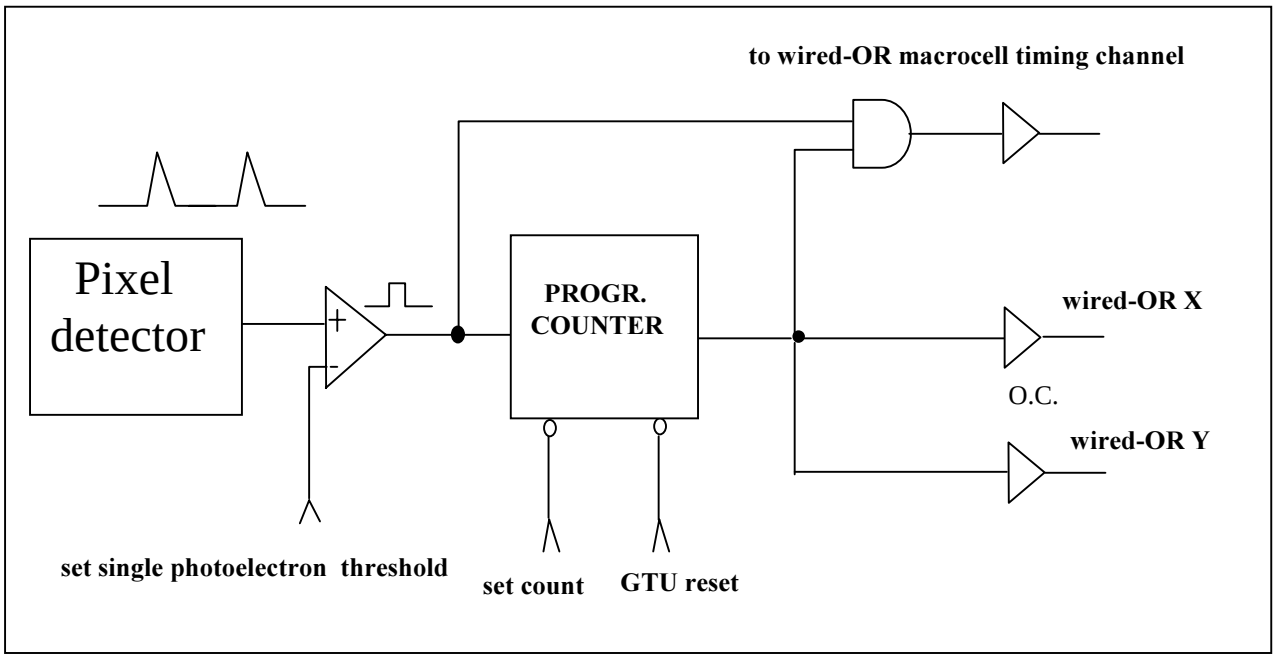

Fig. 3 . Pixel detector front-end.

2.3 Macrocell layout

As figure 4 shows, the Macrocell is organized in rows and columns OR-ing each pixel front-end output. The wired OR of the X rows is routed to the timing and counting channel (one per Macrocell) that will hold in a ring memory buffer single photoelectron arrival time and to a digital counter that will keep the counts per GTU.
The Macrocell is equipped with two ring-memory buffer, one for the X and one for the Y. Information reflecting the status of the rows and columns are written in binary format ("0" / "1"), in those memories sequentially every GTU.
In absence of a trigger signal the ring memory will be continuously written updating the information in memory. At a trigger signal the writing operation stops and the memory are reed backward for an appropriate length given by an gate time unit counter.
The addressing of ring memory is controlled by a 12 bits up/down counter that drives the address bus of the memory for the writing and reading operation.
This particular architecture of the macrocell permits us to reduce the number of read-out position channels. In fact instead of ***n*n*** channels required for an individual-pixel read-out architecture; we have only ***2*n*** channels to read. This is a drastic reduction in the number of position read-out channels. Moreover, the required number of timing channels drop down to one per macrocell.
For sake of clarity we have to say, however, that this configuration is allowed by the fact that we are in the presence of ***single track*** event. The ambiguity introduced by OR-ing X and Y signals, does not interfere with the reconstruction of a track, since signals belonging to the track are coherent in space and time, whereas those that make up the background are incoherent.

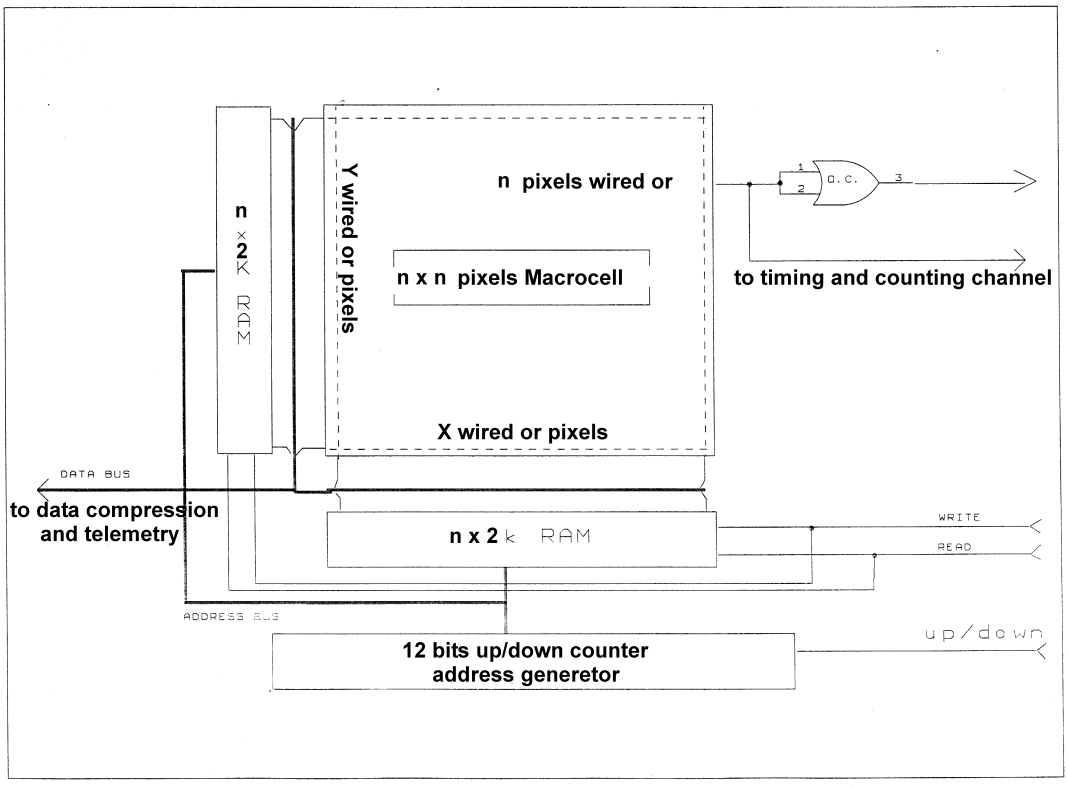

Fig. 4. Macrocell unit.

2.4 Control and trigger module

In figure 5 is shown the control and trigger module. It consists of k*k 8 bit programmable counters and k*k 10 bit counters (one per macrocell), a GTU counter, a pattern-latched register, a microprocessor.

The 8 bit programmable counters count the incoming digitized pulses from the macrocell timing lines and set the correspondent one bit latch pattern if count is above a programmed threshold within a GTU. A total of k*k bit are needed for the pattern register. The information of the pattern register are processed by the microprocessor using an algorithm that compare the previous pattern with the present ones (pipeline mode). If an imposed length condition is met an alert trigger is then generated. The alert trigger enables the GTU counter and the k*k 10 bit counters operation. The event trigger is generated if the GTU counts are within a specified time interval (length of which depends on the physical phenomenon). The read-out will be performed at that event trigger. The k*k 10 bit counters keep track of the macrocells involved in the event and their processed information are used to address a set of macrocells for the read-out cycle.

An important aspect of such design is that the system has the capability of a self-threshold adjustment. In fact it is possible process statistically the information from the pattern register and uses it to set the programmable counter in the pixel front-end at a threshold level obtained from the background itself.

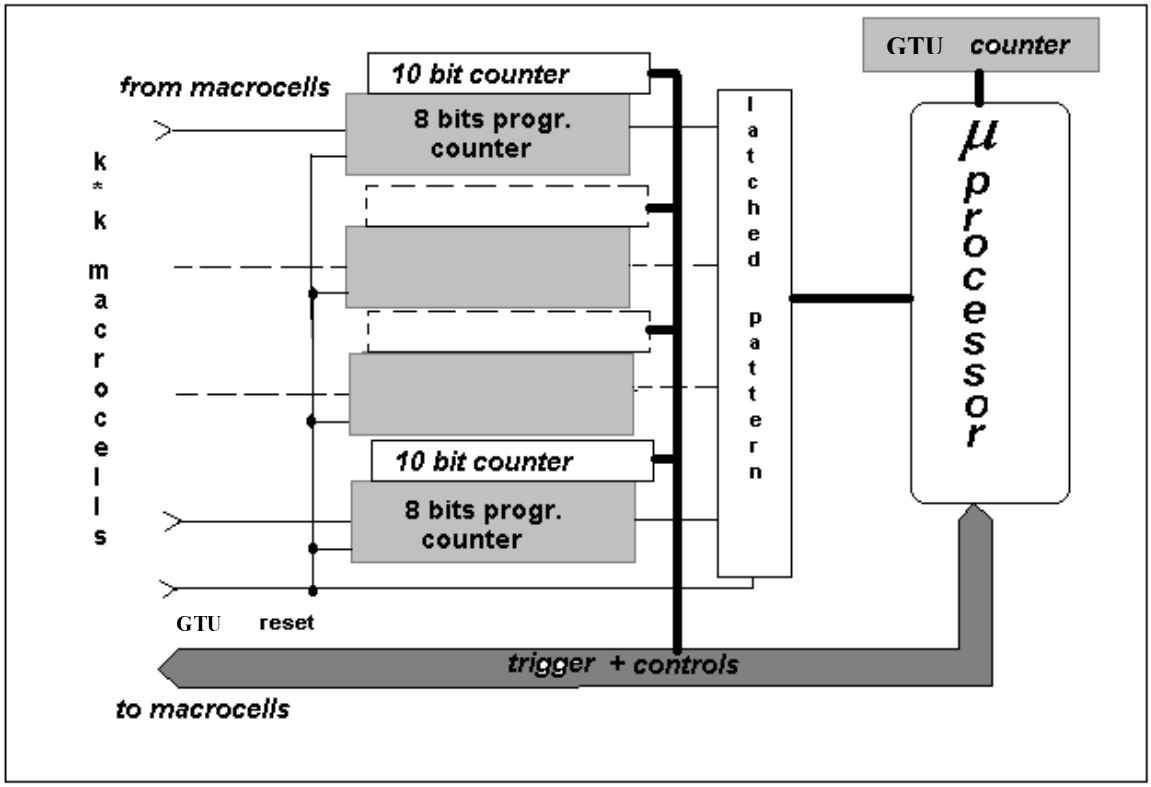

Fig. 5. Control and trigger module.

2.5 Timing channel

Relative arrival time of photoelectrons is recorded by means of logic using passive delay line and ring memory buffers. The implementation of this particular electronics has been developed in our Institute in Palermo and fruitfully installed and operated in EAS ground based experiment in Leeds, UK [2]. The technique consists in write in a ring memory the information coming out from the signal transiting through a multi-tapped 2 ns delay line. With this trick it is possible to record signals with two ns of timing resolution at low cost and high reliability. The timing ring memories are similar for what concern reading to the X and Y position ring memory. The digitized pulses recorded in the memory give the relative arrival time as well as the number of photoelectrons detected in the corresponding macrocell. A sketch of a timing channel is shown in figure 6.

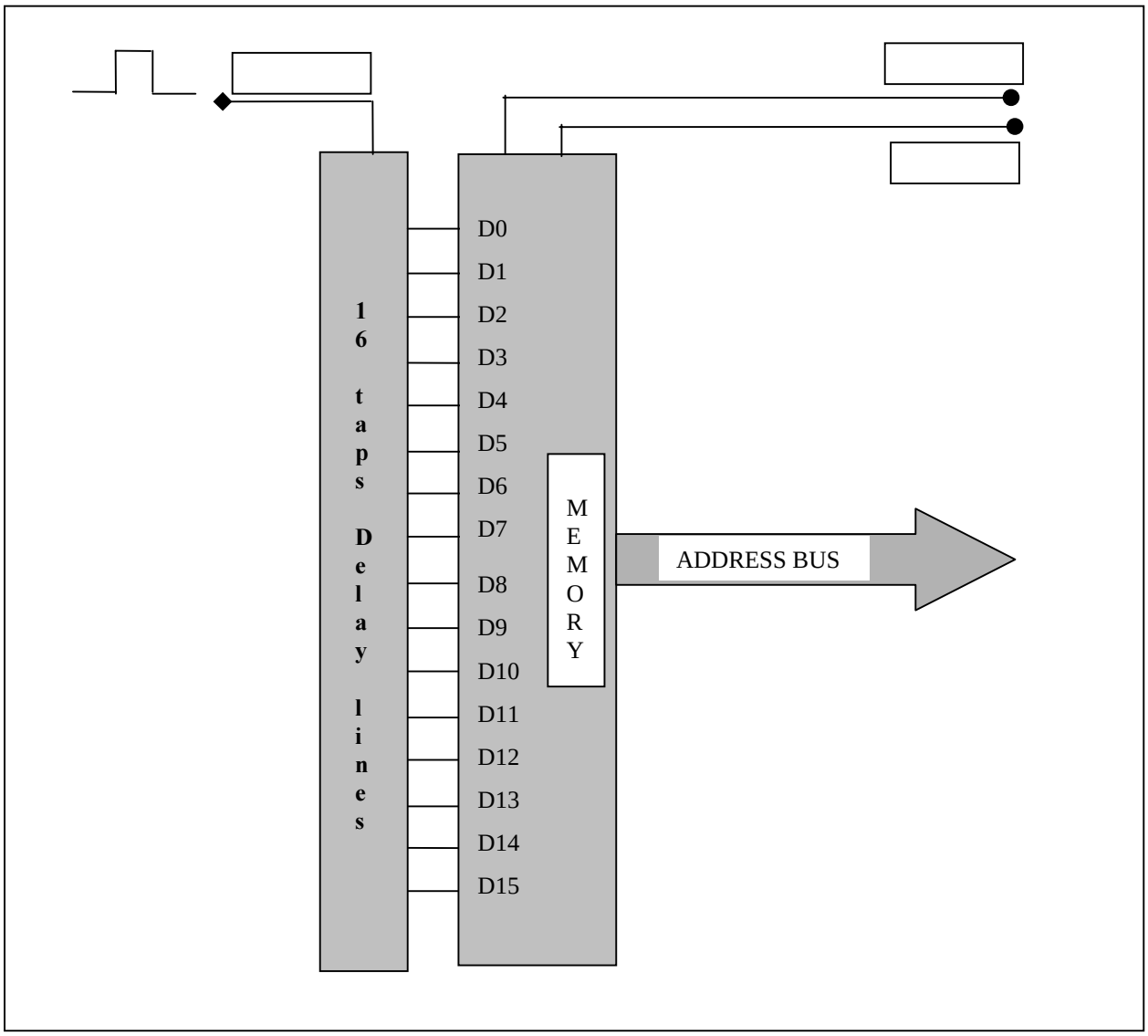

Fig. 6. Timing channel

One timing channel is foreseen for each macrocell in the FIRE design. The digitized pulse signals (10 ns width) coming from the macrocell, OR-ing the rows (or the columns) of the macrocell itself, are sent to the delay lines (2 ns per tap) and the resulting output are connected to the input data lines of the memory that is written with a cycle of 32 ns. This permits to record in binary form the digitized pulses with a resolution of 2 ns. The content of the memories are organized as a sequence of "0" and "1" that represent the logic level of the of the digitized pulse signals. Figure 7 exhibits a partial representation of the memory content in words of the timing channel.

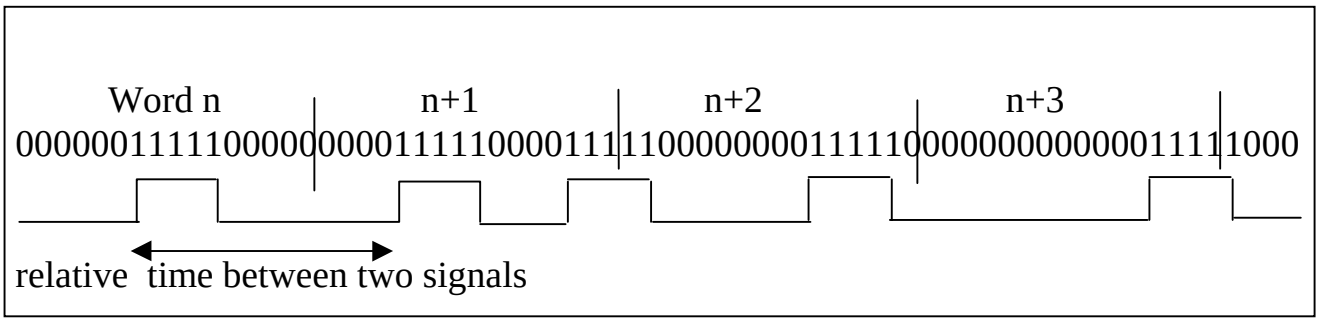

Fig. 7. Pulses representation in the timing channel memory.

With the information recorded in the timing channel and in the X, Y memory position buffers, is possible obtain the relative arrival time of the single photoelectrons and the number of them in each macrocell per GTU. For sake of clarity, we describe the procedure to obtain the photoelectrons number using the X,Y and time information.

Assuming to set, in the individual pixel detector front-end, the set-count line to an integer **m**, we expect that a digitized pulse will pass if **m** or more pulses in the same pixel per GTU are detected. Off line comparison of timing channel content and X,Y memory buffer permit to calculate the total number of photoelectrons belonging to a GTU. Schematic representation of the algorithm is given in figure 8. The lines represent three consecutive GTU's. Full squares are the pixels projected in the X (or Y) view of a macrocell. The three timing diagrams are the content in pulses number of the timing channel in the same GTU.

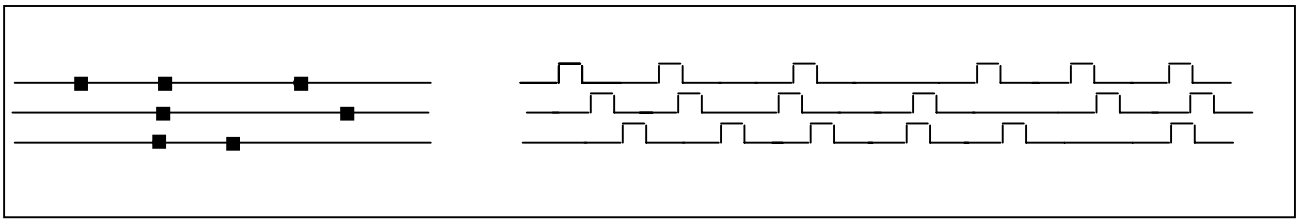

Fig. 8. Schematic representation of three GTU's.

The number of photoelectrons N_{pe} belongs the signal per GTU in the first row is equal to 6, in the second row equal to 7 and in third row equal to 7.
Simple formula for the number of the photoelectrons can be derived:

$$\mathbf{N_{pe} = n_{pulses} - n_{pixels} + m}$$

Where:

$\mathbf{n_{pulses}}$ =total number of pulses in a GTU.

$\mathbf{n_{pixels}}$ = total number of projected pixel in a GTU.

2.6 FIRE block diagram

A simplified block diagram of the FIRE electronics is shown in figure 9. The block diagram summarizes the design concept showing the main modules constituting the electronics proposed. It should also be noted that the simplicity and reliability of a system is very important in spacecraft experiments. The payload, normally, has a limited budget for mass, volume, power and funding. It is necessary to make the best possible use of these budgets in the contest of the mission requirements. The approach used in designing the FIRE system takes into account such requirements and offers a possible solution in term of feasibility to the stringent requirements of such intriguing enterprise.

Design of the FIRE electronics is currently in progress and more detailed electrical schemes will be produced in order to derive the overall characteristic of the system.

Technical and operative feasibility as well as components space qualification availability will be checked and discussed with the industries involved in the project.

Industries have a key role in the success of this project. They must transform our ideas into real and working devices, and often it is not at all easy.

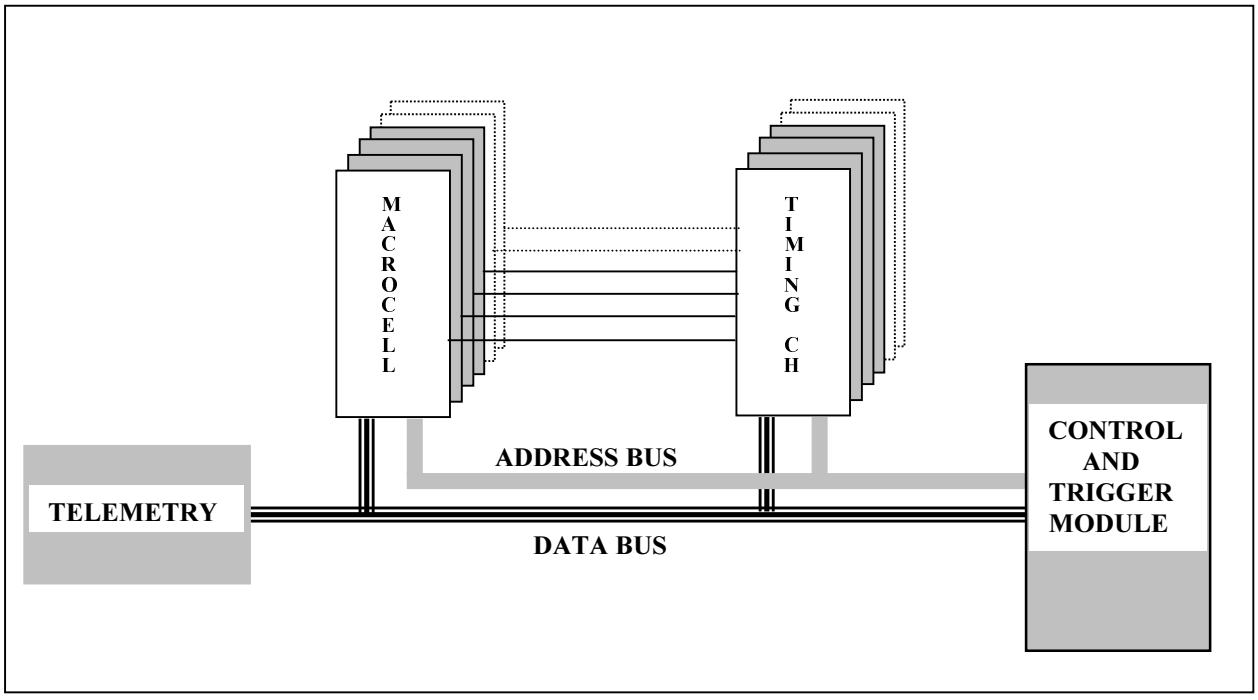

Fig. 9. Block diagram of the FIRE electronics.

3. FIRE SIMULATION AND EVENT SIMULATION

The performance of the entire on-board read-out system has been evaluated with appropriate simulation software. A simulation for the physics aspects involved in the processes has been developed and used to feed the FIRE electronics. The program (hereafter designated "AW") simulate the response of the proposed AIRWATCH FROM SPACE to simulated extensive air shower. AW also generates detailed signal and timing information for all possible event geometry. It takes into account geometrical constraints (pixel size, solid angle, acceptance, ...) and physics factor (shower energy, fluorescence yield, clouds coverage, …) which affect the measurement of an event. Furthermore, AW has been used (and will continue to be used) to test the effect of different height satellite orbit and different optics size on the event rate and shower energy threshold. The goal is, of course, to optimize the system response, taking into account all the possible variables playing a role in the detection of the events.

3.1 FIRE simulation

The assumption used to simulate the FIRE electronics can be summarized in:

- The use of a squared pixel with a size corresponding on the earth of 1Km*1Km .
- The use of a fast detector with a resolving time ≥ 10 ns (parameterized).
- The use of a macrocell of 48*48 pixels.
- The use of a focal plane detector constituted by 25 macrocells (240*240 pixels).

The behavior of the individual pixel detector front-end, for the background, has been simulated calculating the poissonian probability to have ≥**m** photoelectrons in one pixel per GTU and multiplying it for the total number of pixels (240*240). UV photons, belong to the shower, are also converted in photoelectrons and then used as input to the pixel detector front-end. More on this aspect will be said in the part treating the event simulation. The timing channels contain, presently, the total count (background + signal) per GTUit of each macrocell of the focal plane. Simulation of the timing channel as proposed in section 1, will be inserted later on.
Each macrocell is represented by a matrix of 48*48 bits. The X and Y wired-or connection is realized calculating the positions of the hit pixels (background and/or signal) in the matrix in a GTU and writing the binary status of the pixels ("1"=hit, "0"=not hit) to the correspondent two matrix $X_{x,f}$, $Y_{y,f}$ (with x=X position, y=Y position and f =GTU number) at any GTU. This operation involves all the 25 macrocells forming the focal plane detector. As results of this architecture the 25*2 memory matrix maintain, separately, the story of what was happened previously before that the event trigger stops the memories writing. The information kept in the memories is the imaging of the hit position in the X and Y view. Figure 10 shows a sketch of a such configuration.

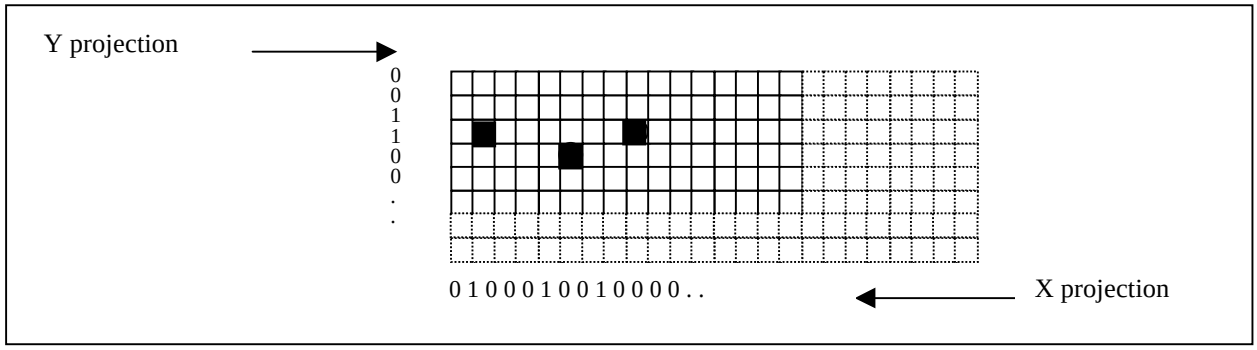

Fig. 10. Squares represent pixels and full squares hit pixels.

From the information given by the X and Y projection (implicitly GTU correlated) it is possible to reconstruct the event, whereas from the content of the timing channels (number of photoelectrons) is possible to estimate the energy of the event. Section 3 contains detail of some typical events.

The control and trigger module has been simulated taking into account the characteristic described in section 1 (Control and trigger module). An algorithm has been implemented, using the information of the simulated pattern register, to generate an event trigger. This algorithm uses the logic status of the bits constituting the pattern register. The algorithm applies a recursive “bit-wise AND” operation on the changing content of the pattern register until a condition of at least three occurrences over a set threshold, calculated averaging the sum of the twenty-five 8 bit programmable counters, is found in the same macrocell. Table 1 shows synthetically the algorithm used.

Table 1.

Pattern	AND buffer	occurrences in the same colums (macrocell)	
1 0 1 0 0 0 0 0			
0 1 0 1 0 0 0 0	0 0 0 0 0 0 0 0	0	
1 0 0 0 0 1 0 0	0 0 0 0 0 0 0 0	0	
1 0 1 0 1 0 1 0	1 0 0 0 0 0 0 0	1	
0 0 1 0 0 1 0 0	0 0 1 0 0 0 0 0	1	
1 0 0 1 0 0 1 0	0 0 0 0 0 0 0 0	0	
0 1 0 1 0 1 0 0	0 0 0 1 0 0 0 0	1	
0 0 1 1 0 0 0 0	0 0 0 1 0 0 0 0	2	
1 0 1 1 0 1 0 1	0 0 1 1 0 0 0 0	3	trigger alert
0 1 0 1 0 0 1 0	0 0 0 1 0 0 0 0	4	
. . . . .	. . . . .	.	
. . . . .	. . . . .	.	
0 1 0 0 0 1 0 0	0 0 0 1 0 0 0 0	0	event trigger generated
0 0 1 0 1 0 0 0	0 0 0 1 0 0 0 0	0	if track length condition is met

As the condition is met (trigger alert) the GTU counter begin to be increased. Contemporarily the twenty-five 10 bit counters begin to accumulate counts from the macrocells.
When the occurrences drop down to the set threshold the GTU counter is stopped and it is compared to the expected characteristic range of the track length. If the condition is not met the GTU counter as well as the accumulation counters registers are reset and the operation continues. If the condition is met the event trigger stops the memories writing operation after some few GTU and stops also the accumulation counters.
Now it is possible using the information of the accumulation counters to address the macrocells that exhibit the maximum count and the three relative ones. The memories are reed back for the number accumulated in the GTU counter plus a judicious amount of GTU and then transferred in the data telemetry buffer.

3.2 Geometry and coordinate system

In order to simulate shower, is needed to define a coordinate system. Figure 11 shows the coordinate system adopted.

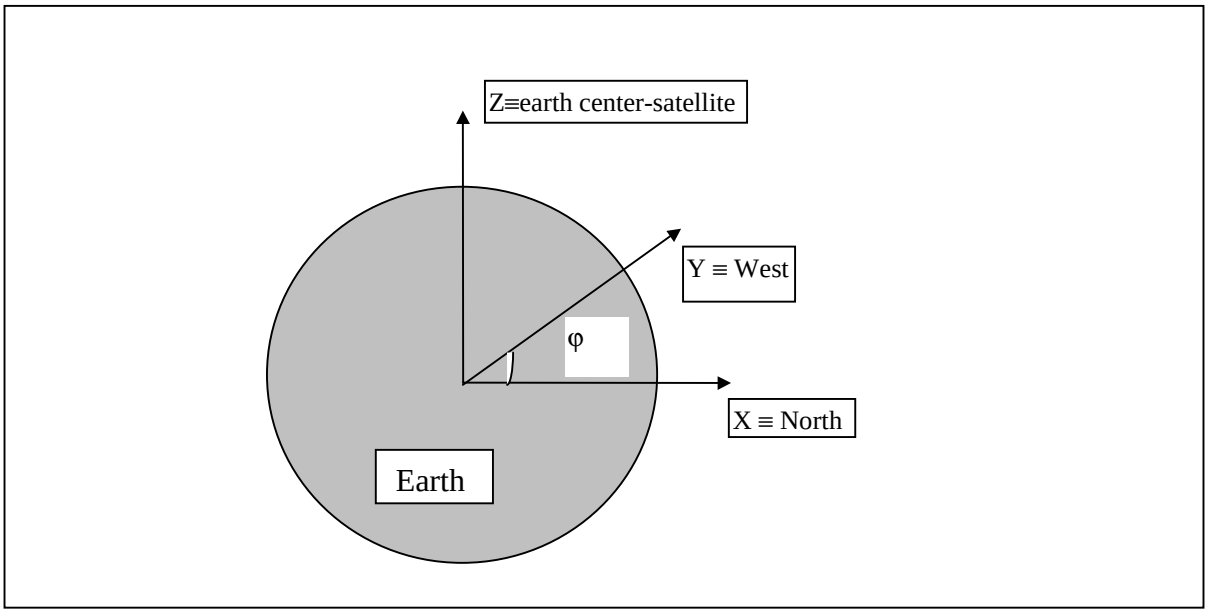

Fig.11. AIRWATCH coordinate system.

Showers are synthesized with random geometric parameters taking into account the geometry of the Earth and atmosphere intercepted by the field of view. Figure 12 shows a sketch of the ROS and the geometric parameters involved in the simulation. We adopt, in the event simulation, a couple of Fresnel lenses with a total angular aperture of ±30° (see appendix A) [3].

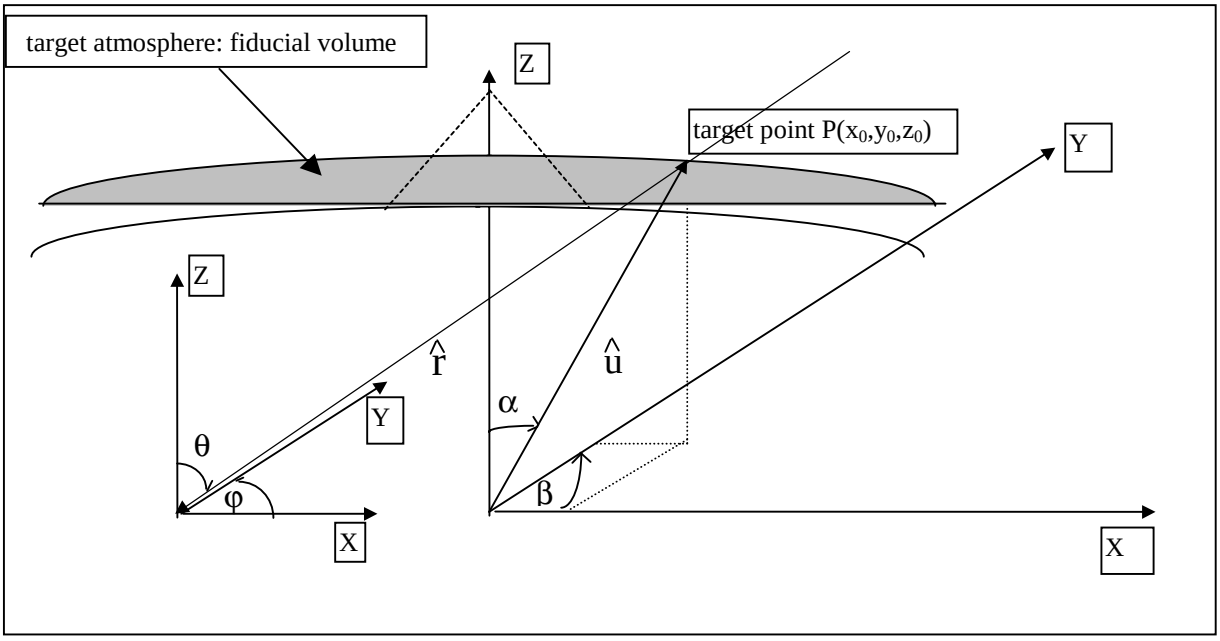

Fig. 12. Sketch of the Earth-atmosphere ROS.

3.3 Event simulation.

Event simulation has been developed to estimate counting rate, angular and energy resolution. Showers are simulated taking into account geometric parameters θ, ϕ, α, β defined in figure 11 and X, the depth of penetration of the primary cosmic ray into atmosphere. Keeping the number of showers generated per unit solid angle a constant requires that the geometrical parameters θ, ϕ, α, β be distributed proportionately to $dAd\Omega = R_t \sin\alpha\, d\alpha\, d\beta\, \cos\theta\, d\phi$. This means distribute uniformly on the part of the sphere of radius R_t=R+h (with R=earth radius and h=50 Km thickness of the atmosphere) and spherical-cup height h, the entry points (target points) of the primary particles (vector **u)**. Then distribute the direction of the tracks (produced by showers: vector r) proportionately to $\cos\theta\, d\phi$. Using rejection method it is possible select events landing inside the surface seen by the F.O.V.. This is accomplished by calling a random number between 0 and 1 and generating parameters such that:

$\alpha = 1/12.59 * \cos^{-1} y_1$	$0 \le \alpha < 0.03972\ \pi$
$\beta = 2*\pi*y_2$	$0 \le \beta < 2*\pi$
$\theta = \cos^{-1} y_3$	$0 \le \theta < \pi/2$
$\varphi = 2*\pi*y_4$	$0 \le \varphi < 2*\pi$

the α and β angles are used to find the target point $P(x_0,y_0,z_0)$:

$x_0=(R+h)*\sin\alpha*\cos\beta$
$y_0=(R+h)*\sin\alpha*\sin\beta$
$z_0=(R+h)*\cos\alpha$

where R=6378.14 Km earth radius
and h=50 Km atmosphere thickness

the value of α has been chosen taking into account the curvature of the earth.

The θ and φ angles are used to find the vector **r** imposing the condition to pass for the point $P(x_0,y_0,z_0)$ such that :

$x-x_0=l/n\ (z-z_0)$ (1)
$y-y_0=m/n\ (z-z_0)$ where $l=\sin\theta*\cos\varphi$
$m=\sin\theta*\sin\varphi$
$n=\cos\theta$

Now resolving the system of three eq. and three unknown x,y,z we find the intersection point on the surface seen by F.O.V.

$$\begin{cases} x^2+y^2+z^2=R^2 & \text{where R=earth radius} \\ x-x_0=l/n\ (z-z_0) \\ y-y_0=m/n\ (z-z_0) \end{cases}$$

Resolving for z we have:

$a*z^2-b*z+c=0$

where $a=(l/n)^2+(m/n)^2+1$
$b=2*[(l/n)^2+(m/n)^2]*z_0-2*l/n*x_0-2*m/n*y_0$
$c=[(l/n)^2+(m/n)^2]*z_0^2-2*[l/n*x_0-2*m/n*y_0]*z_0+x_0^2+y_0^2-R^2$

with solution given by:

$z=(b\pm\sqrt{b2-4*a*c})/(2*a)$

the solution to consider is the one with $(b+\sqrt{b2-4*a*c})/(2*a)$
Finally x and y are found substituting the z value in the system (1).

As an example figure 13 shows the zenith angle distribution of simulated showers directions landing inside the FOV. obtained considering only geometrical contribution.

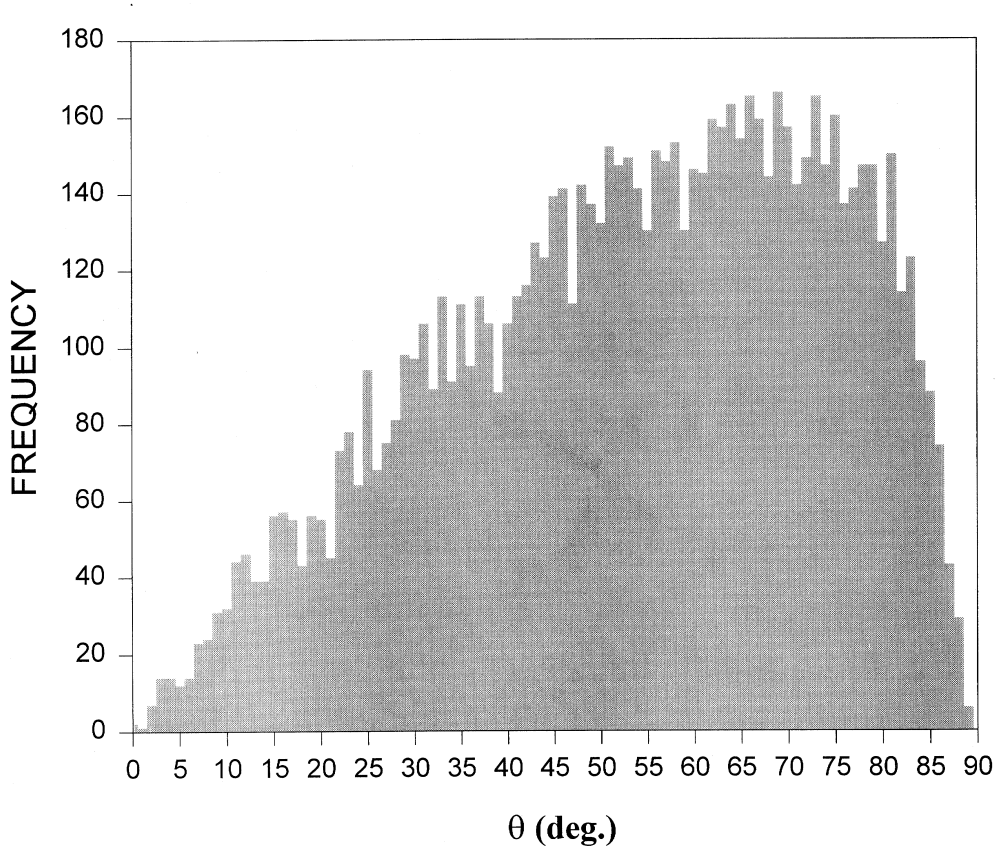

Fig. 13. Expected zenith angle distribution of tracks landing inside FOV.

Longitudinal development of the shower is calculated by using the Il'ina parameterization formula [4]. The formula calculates the number of electrons N_e at different observational depth level of the shower in function of the primary energy (see appendix B).

Standard model of the atmosphere has been included in our calculation that takes into consideration the temperature dependence of altitude and consequently, the scale height variation with altitude (see appendix C).

The shower generated with the random parameter θ, ϕ, α, β is propagated into atmosphere in steps of ΔL=250 meters. The 250 m step (transformed coherently in g/cm^2) is in agreement with GTU chosen of t=833 ns. For any of those steps, the x,y positions of the pixels hit are calculated and used for recording, in the correspondent pixel location, the number of background photons as well as N_e .

The N_e is converted in photoelectrons number N_{pe} , using the parameterization:

$$\mathbf{N_{pe} = N_e * Y_p * A * k_1 * k_2 * k_3 * k_m * \Delta L / 4*\pi*H^2}$$

with:
N_e : Number of electrons (within ΔL) calculated using Il'ina parameterization.
Y_p: Yield of photons = 4.7/m/electron (constant).
A : Acceptance area of the lens; (parameterized)
K_1: Transmission coefficient in Ozone layer = 0.58 (constant; see appendix D).
K_2: Transmission coefficient in the atmosphere = 0.75 (constant).
K_3: Quantum efficiency of the sensor = 0.25 (constant).
K_m: Diffraction efficiency of the two lenses (including filter) = 0.81 (constant).
H : Height of satellite (parameterized).
ΔL: track path length = 250 m (constant).

The number of photoelectrons obtained from the above formula is fluctuated according to the Poisson statistic and recalculated allowing for CRT (parameterized). Background photoelectrons, $\mathbf{N_{bg}}$, are also generated in the same GTU using the following formula and then fluctuated around the mean value:

$$\mathbf{N_{bg} = <B> * A * k_1 * k_2 * k_3 * k_m * \Delta\Omega * t}$$

With:
<B>: Average background photons = 100 photons/m^2 sr ns (see appendix A).
$\Delta\Omega$: Pixel solid angle (parameterized). Pixel size is assumed 1 Km* 1 Km.
t : GTU=833 ns (constant).

The single shower simulation stops when the shower has reached the sea level altitude. Cloud coverage level has been introduced in the AW program as a parameter for allowing a more complete study of the experimental response to the possible different climate conditions.

4. Analysis of simulated events

As Aw program has been realized using graphic representation, we would like to show and explain a typical event display before to show statistical analysis of the simulated events. The matrix in the event display represent 240*240 pixels organized in 25 macrocells each of 48*48 pixels. The event display is the graphic representation of the parameters involved in the simulation. A single event display actually consists of several screen windows that synthesize in visual way the more interesting parts of the analysis. Moreover, runtime setting of some key parameters permits to understand straight away the response differences to the changed parameter values. We will show only a few screen windows of such event display hoping that such graphic representation could be helpful in the comprehension of both FIRE system and physics phenomena.

4.1 Event display

A typical simulated event of 10^{20} eV is shown in figure 14. This first picture of the event display shows the graphics representation of a track produced by a shower of 10^{20} eV with zenith angle of 72.34 deg. and azimuth angle of 229.9 deg.. The track has been represented filling the correspondent pixels when the signal is above the set threshold.

Input parameters as well as output values are shown for completeness.

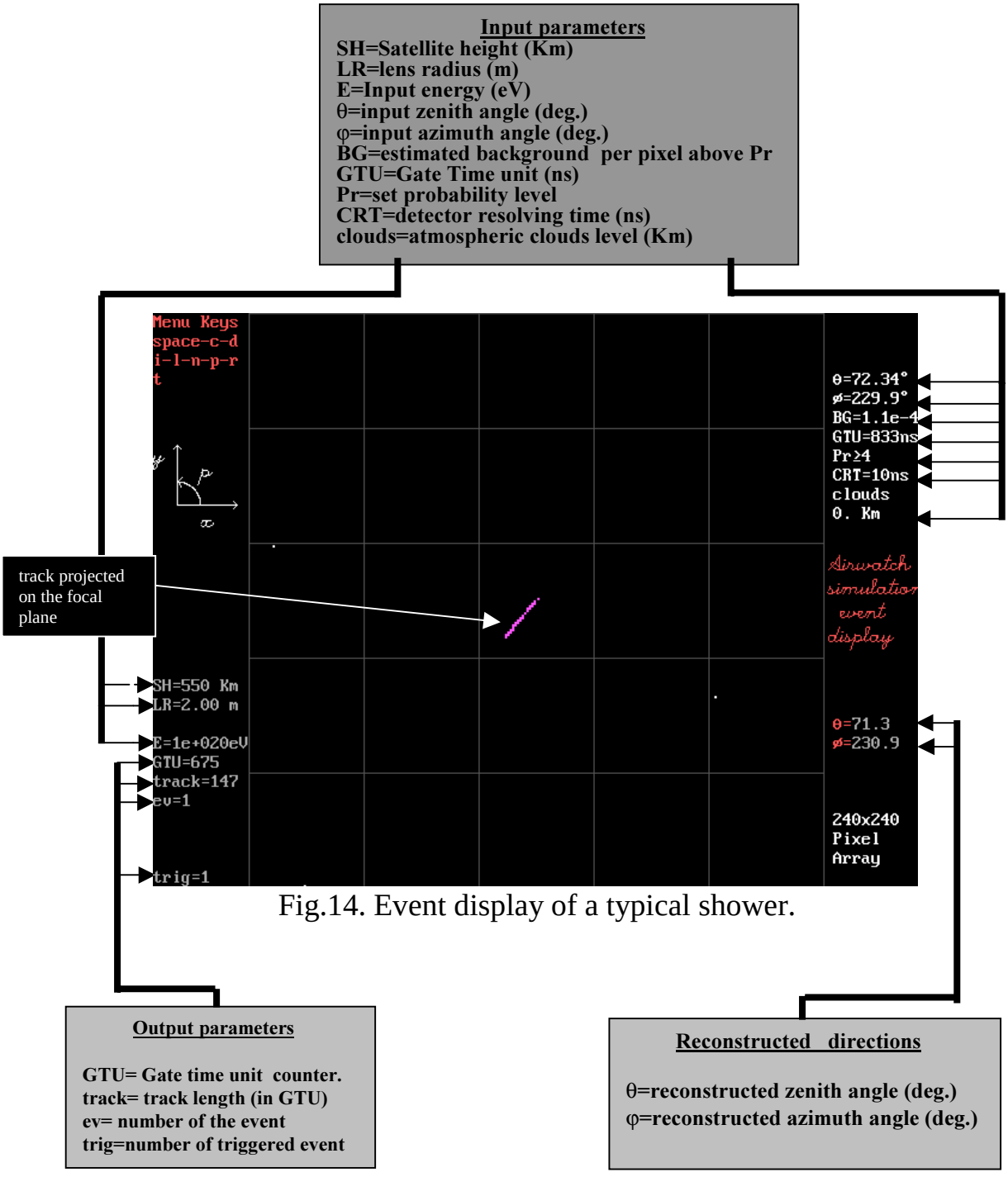

Fig.14. Event display of a typical shower.

Figure 15 shows the accumulated photoelectrons in the macrocells in form of a histogram. The higher bar belongs to the macrocell interested by the track and background whereas the others contain the background. Such representation explains how is easy identify one or more macrocells in which the track is present. Moreover, the identification macrocells number is used to form the address for the read-out operation to be performed at the event trigger.

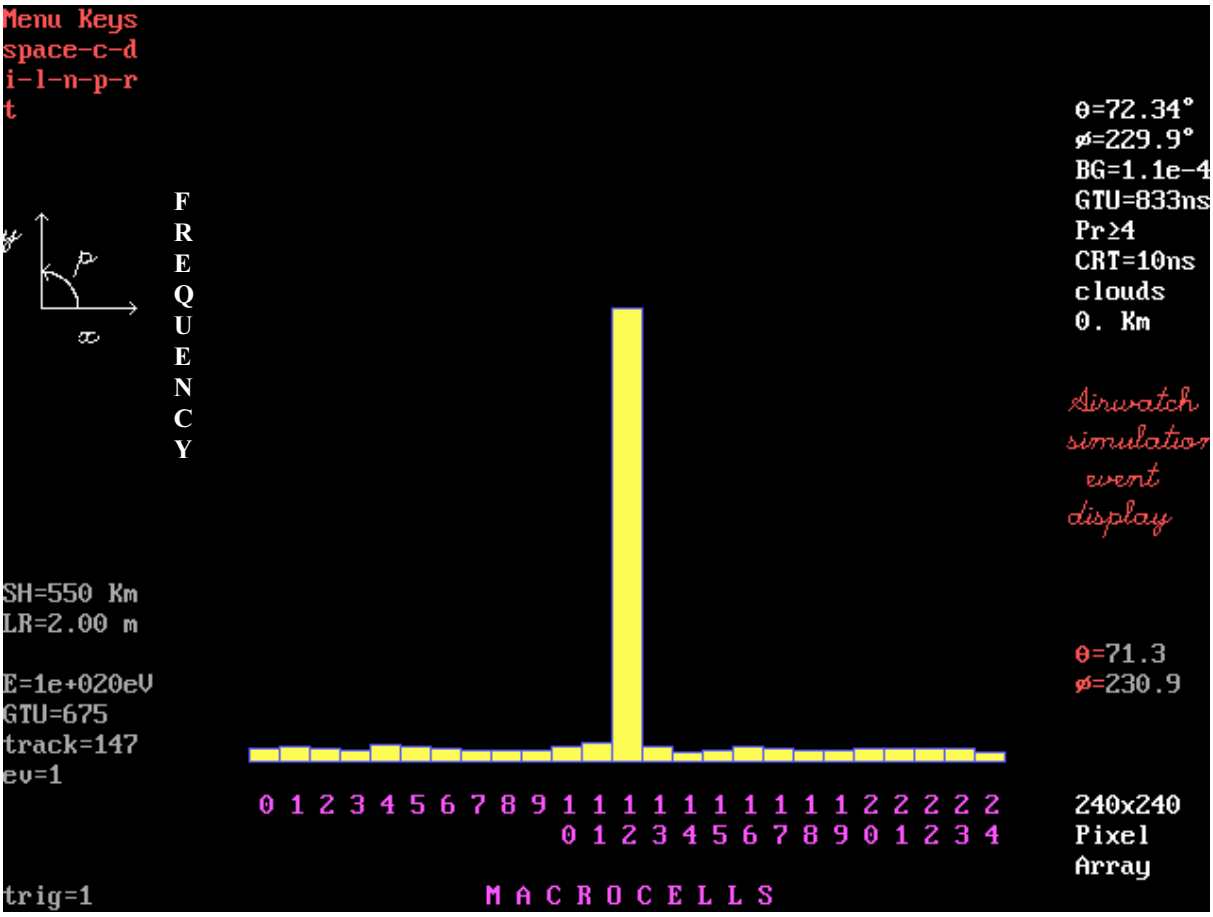

Fig. 15. Signal and background accumulated in the 10 bit counters.

As is shown in the figure 16 the track and the background in both projections are represented. The ordinates are in GTU. This graphic has been obtained, simply, representing graphically the contents of the position (X,Y) memory buffers in sequential order of GTU. The figure shows also three other macrocells that exhibit the three higher relative maxims. Such criterion has been adopted to allow the reconstruction of tracks belongs more than one macrocell (we recall the each macrocell work independently to the others: see examples in appendix D). From the analysis of both the projections and GTU information it is possible to reconstruct the zenith and azimuth angles by means of simple mathematics.
Calling with x the portion of identified track on the X projection and with y the portion in Y projection:

$\varphi = \tan^{-1}(y/x)$

$\theta = 2\tan^{-1}((P/c*t)*\sqrt{x^2+y^2})$ with t=GTU and P=pixel side (1 Km)

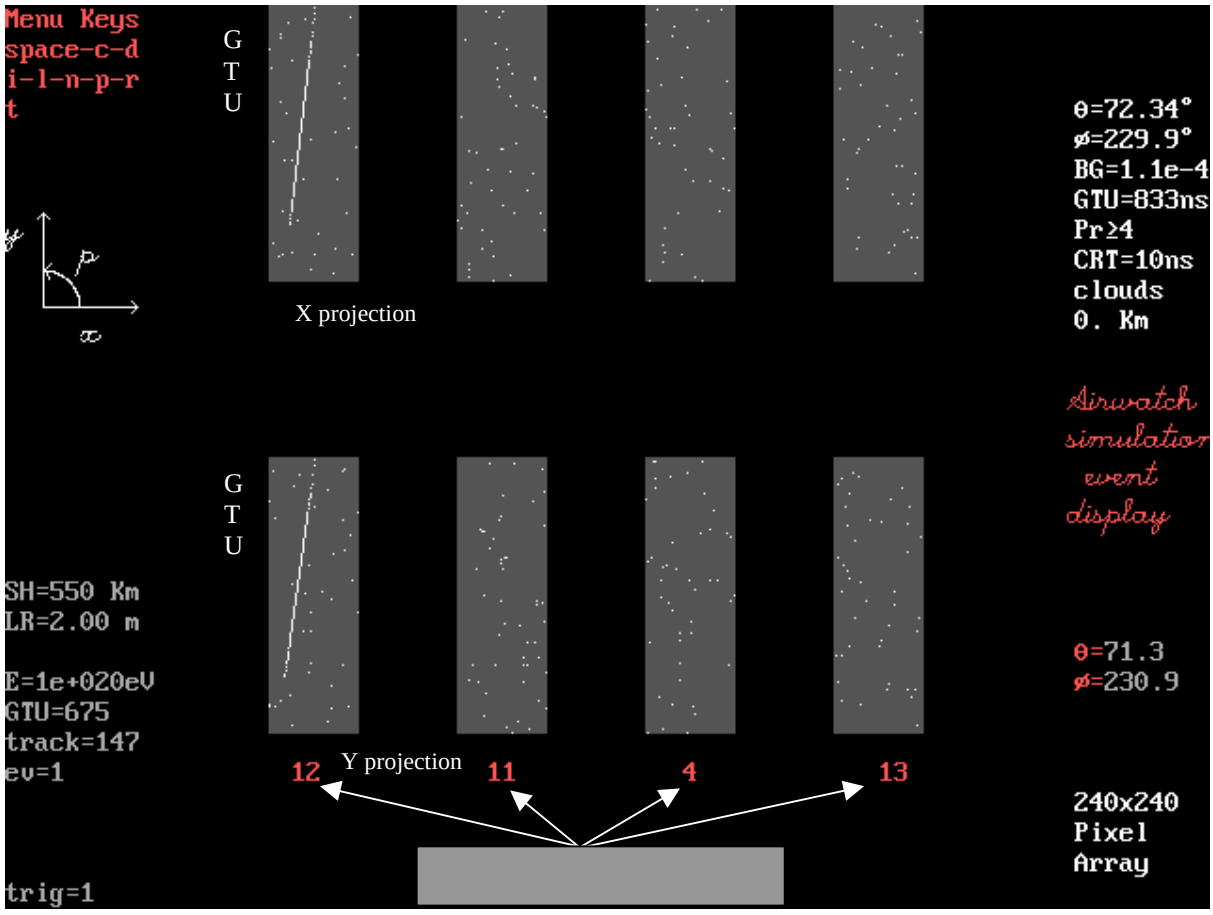

Fig. 16. Track representation in X and Y projection.

Figure 17 and 18 show the representation of the shower profile as calculated by AW simulation program. Figure 15 and 16 differ only for the different ordinate scale, being one logarithmic and the other linear. The brighter part of the curves represents the part of the shower profile detected. The graphic shown at the bottom of both the figures has a further ordinate that indicates the number of photoelectrons detected at the abscissa slant depth. The meaning of the scattered points shown in the bottom graphics is given in the picture itself. Are represented graphically also the ground and clouds level.

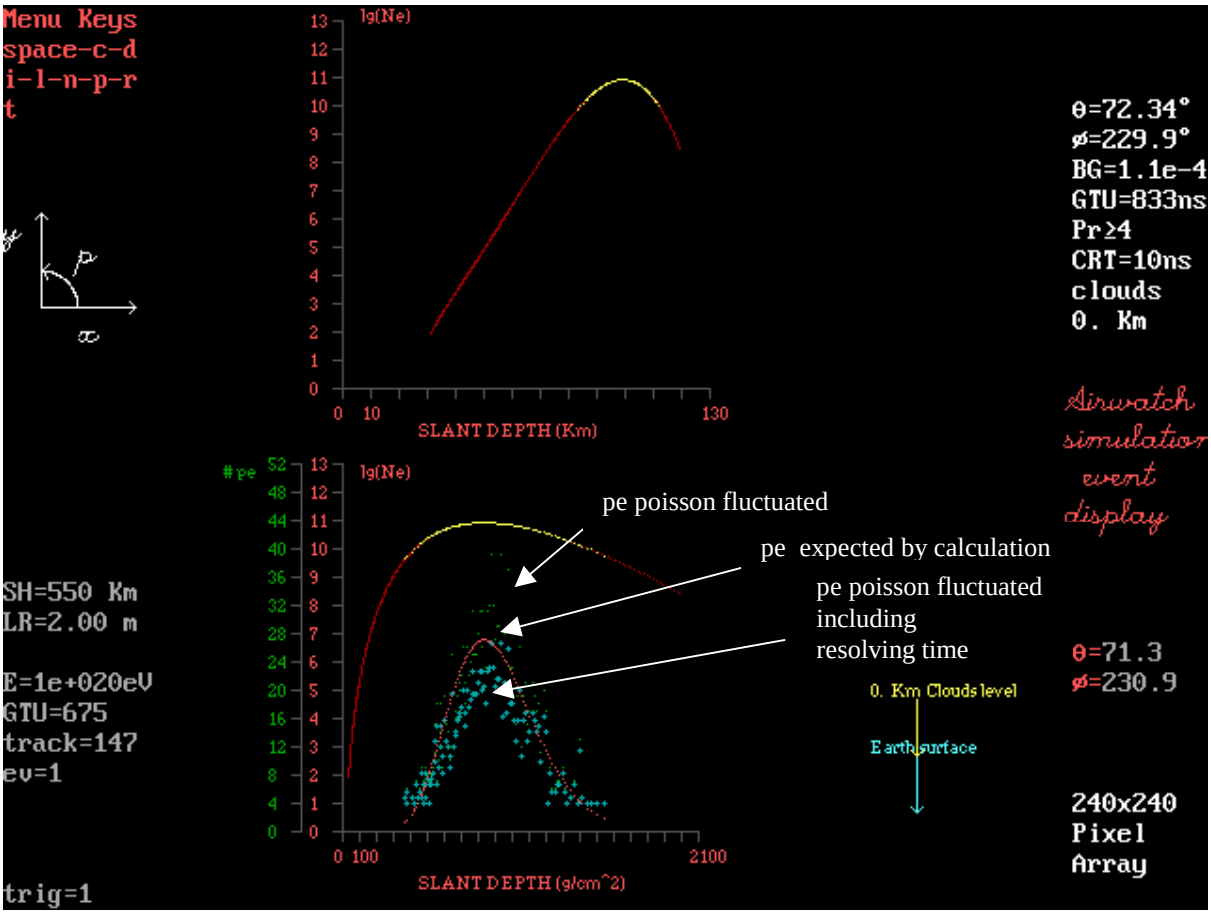

Fig. 17. Shower profile representation.

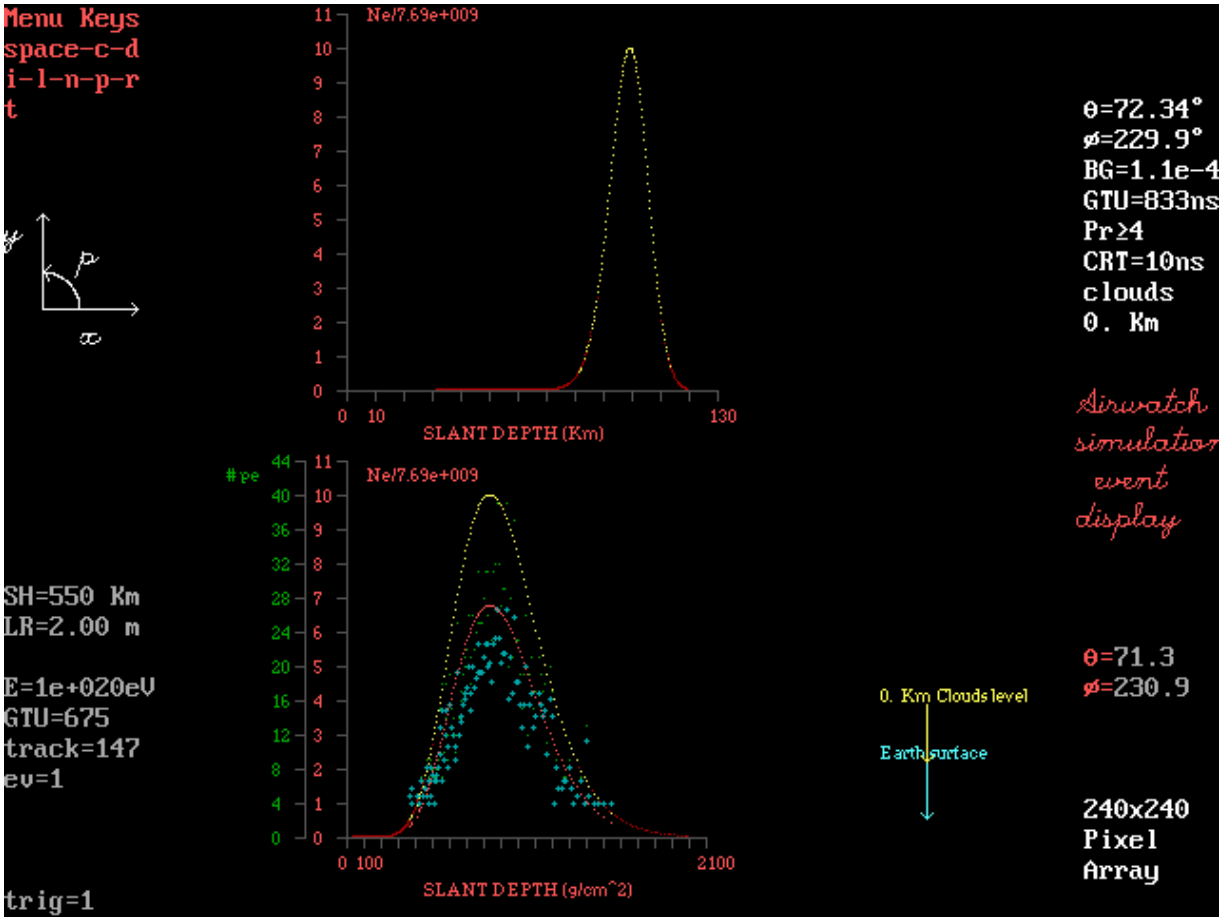

Fig. 18. Shower profile representation.

Figure 19 shows the representation in form of a histogram of the number of photoelectrons per GTU (path length= 250 m). The upper part of the figure shows a sequence of little boxes (pixels) that symbolize the track. In realizing such track we have used the following convention:

- The boxes are drowned horizontally if the same pixel has been hit in successive GTU's.
- The boxes are drowned vertically if the pixel hit is different from the previous ones.
- Empty boxes have drowned if signal is below the threshold.

A line representing the background level is also shown in the picture.

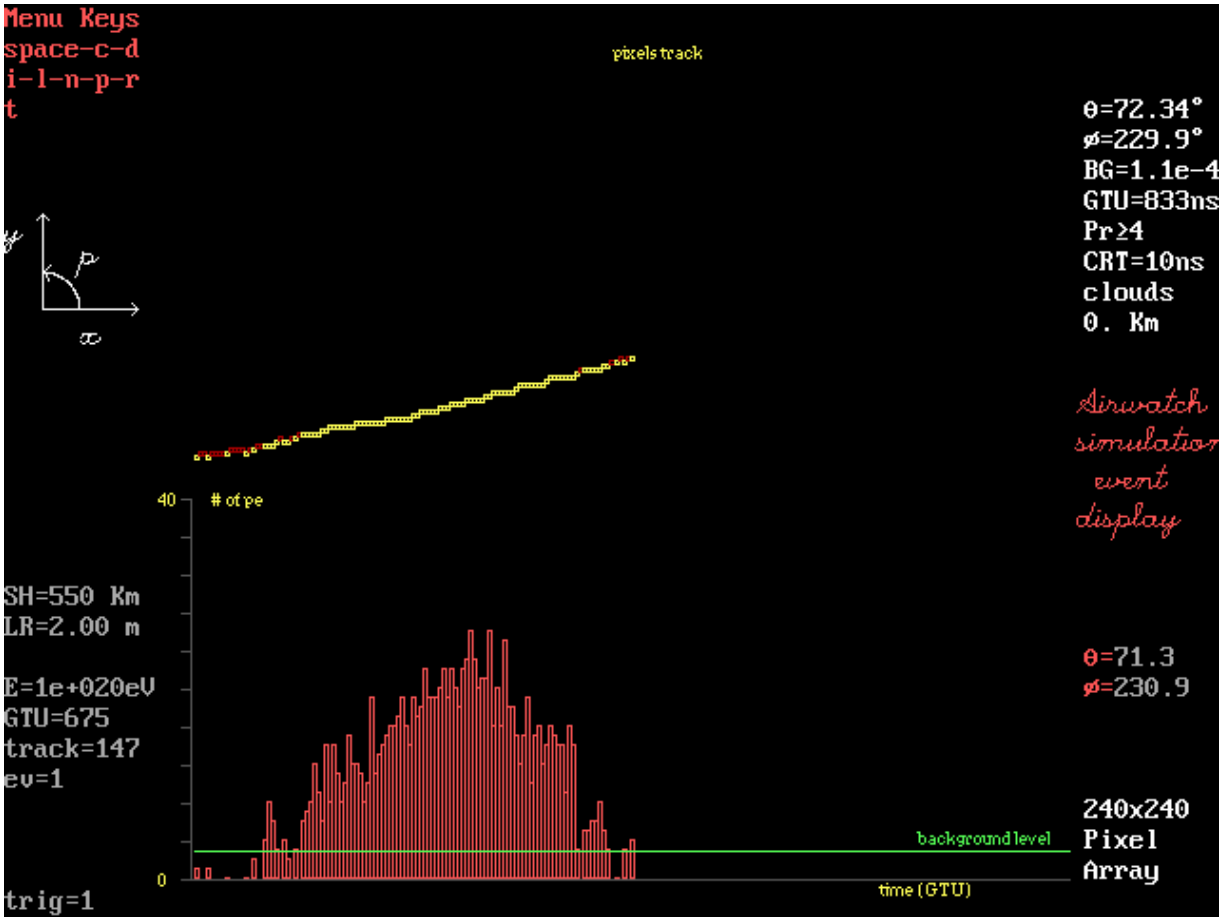

Fig. 19. Histogram of photoelectrons belong a track.

4.2 Statistical analysis of simulated events.

In order to calculate effective trigger aperture, angular resolution and rates, AW determines the minimum energy **E** which a shower of specified geometry must have in order to produce a sequence of signals in the focal plane detector (pixels).

One of the simplest schemes we have used thus far requires that the shower profile must be detected starting approximately from the 25% of the trailing edge to the 25% of the leading edge of the shower curve. In presence of clouds we have limited the detection of the leading edge to 60%, allowing thus the reconstruction of the maximum of the profile. In this analysis we consider showers landing inside the ROS intercepted by the FOV. However, also with this limitation, the trigger aperture of the proposed " Airwatch from Space" is of the order of a factor 20 bigger than the stereo HiRes Fly's Eye trigger aperture [5]. A greater value (≈ a factor 2) must be expected for the effective trigger aperture if we consider instead the fiducial atmospheric volume intercepted by the F.O.V..

4.2.1 Trigger aperture

Figure 20,21,22 and 23 show the effective trigger aperture for the four analyzed configurations. These configuration, that take into account satellite height orbit and size of Fresnel lens as well as ***constant*** clouds level, have been chosen for estimating the corresponding response of the system to a realistic operational mode. It should be recalled that in simulating the events we have kept constant the optics aperture (±30°) and the quantum efficiency of the detector (25%).

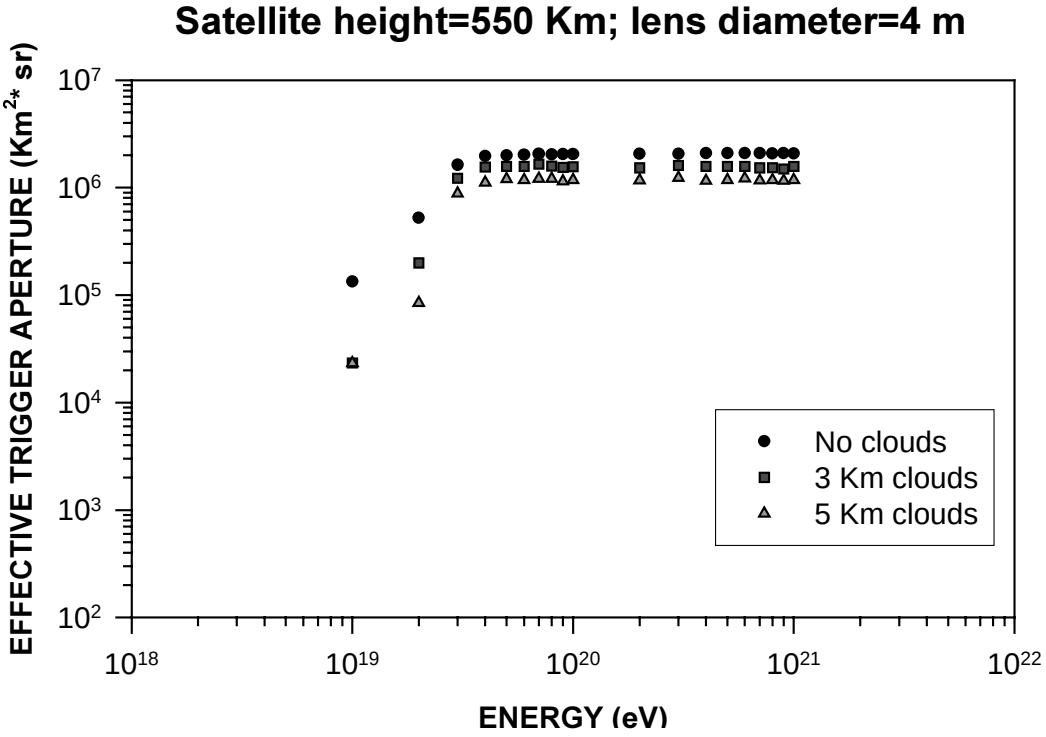

Fig. 20. Effective trigger aperture variation with primary energy. Satellite height=550 Km. Lens diameter 4 m.

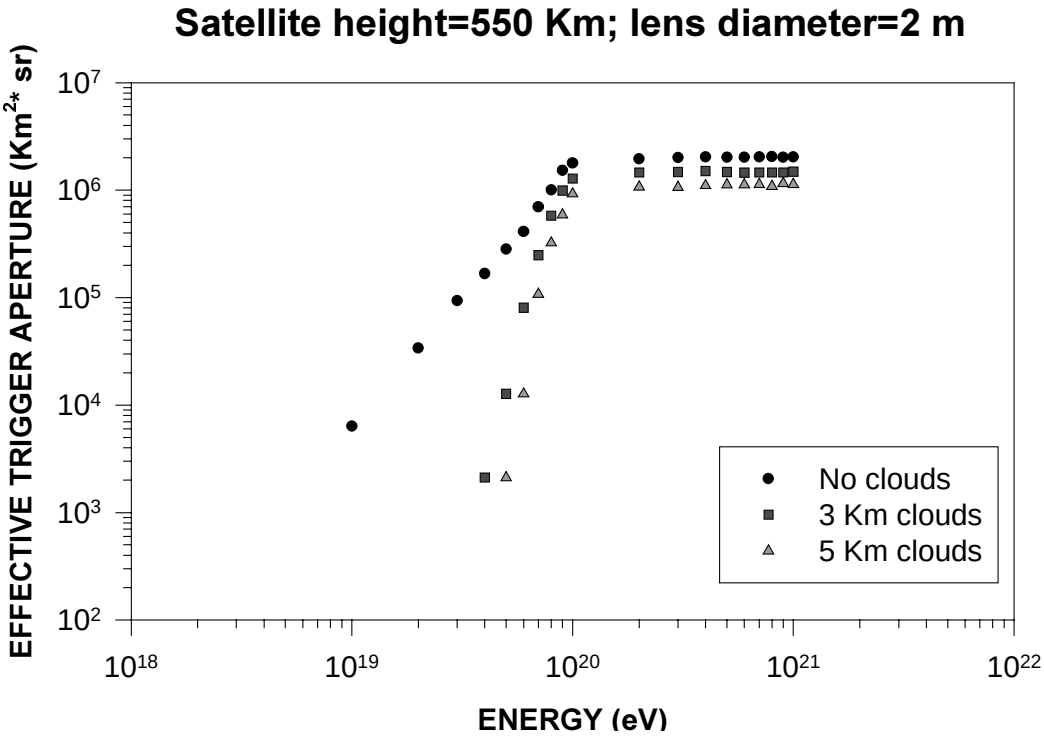

Fig. 21. Effective trigger aperture variation with primary energy. Satellite height=550 Km. Lens diameter 2 m.

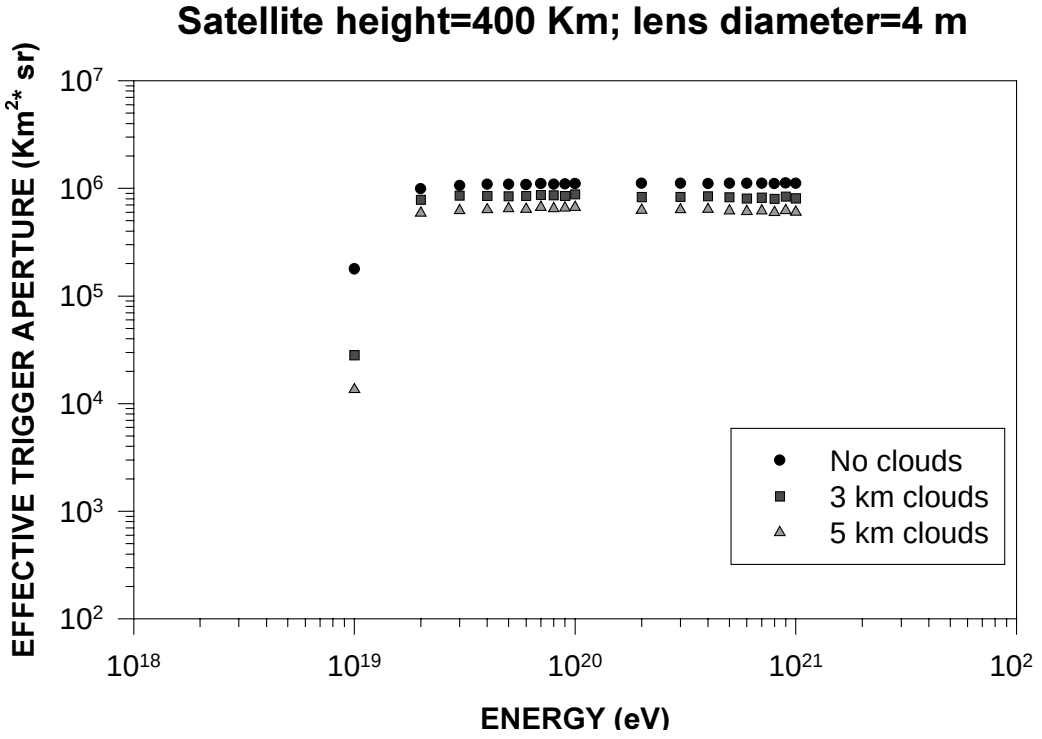

Fig. 22. Effective trigger aperture variation with primary energy. Satellite height=400 Km. Lens diameter 4 m.

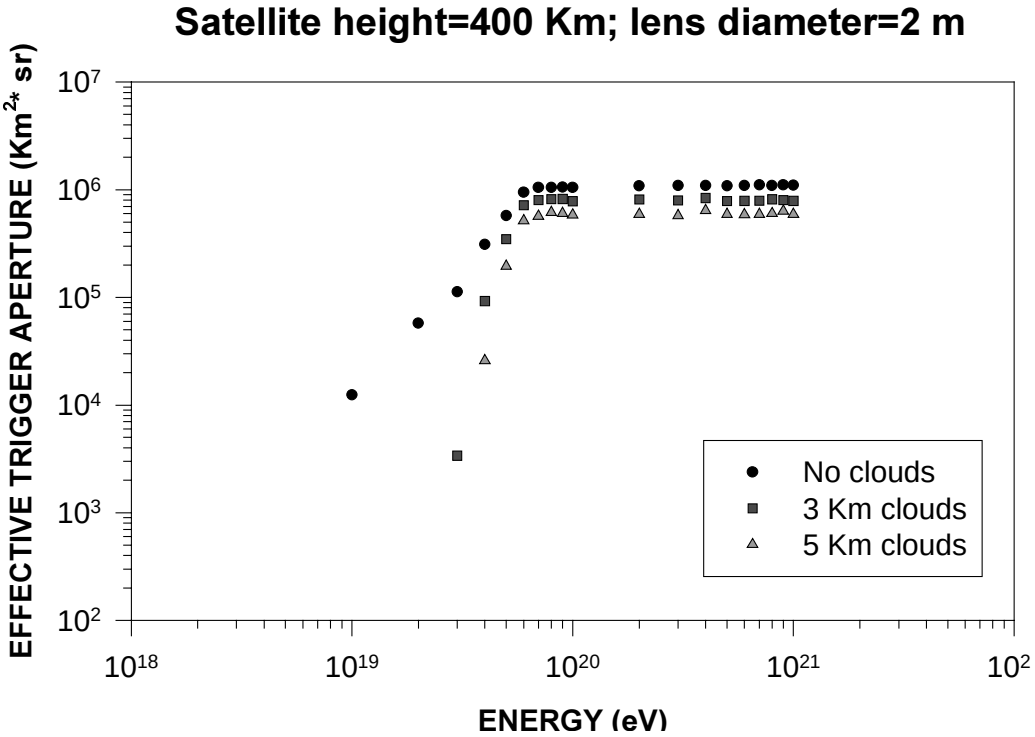

Fig. 23. Effective trigger aperture variation with primary energy. Satellite height=400 Km. Lens diameter 2 m.

4.2.2 Zenithal angular resolution

As the angular resolution is track length dependent, we expect that for the more inclined tracks the angular resolution improve. This is evident in the figures 24, 25,26 and 27 that show the differences between input simulated zenith angle and reconstructed zenith angle $\Delta\theta$ in terms of standard deviations for the four configurations simulated.

The 2 π solid angle aperture has been divided in 6 equal size bins to study the effect of the tracks inclination and primary energy on the zenith angular resolution.

Figures 24, 25, 26, and 27 show the binned zenith angular resolution in absence of clouds, with 3-Km and 5-Km cloud coverage. As is clear from the graphics, without clouds all the solid angle bins are well resolved whereas with 3-Km and 5-Km cloud coverage, the tracks (around the maximum of the shower profile) are partially hidden forbidding the detection of those showers with zenith angle less of 47 degrees and 58 degrees respectively.

However no strong effect on the angular resolution due by the clouds coverage has been found for all the class of detected events.

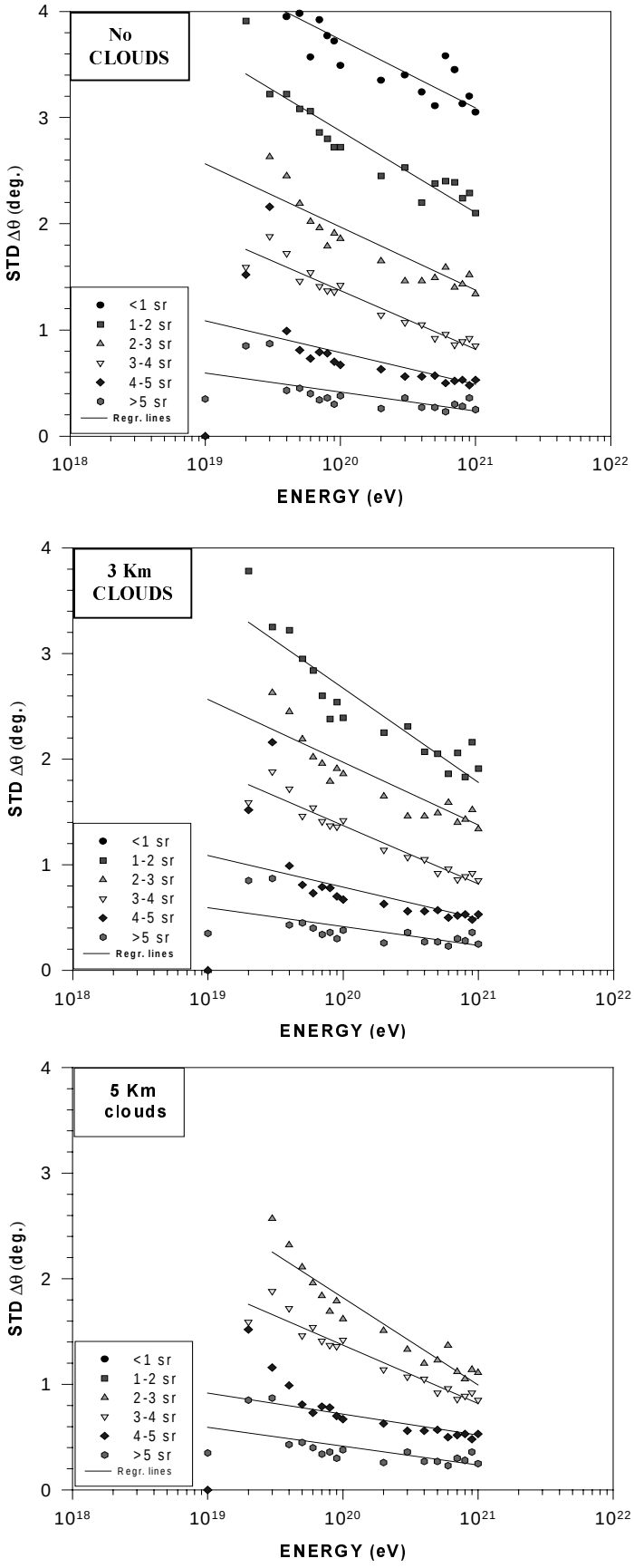

Fig. 24. Zenith angular resolution at different solid angle bins. Satellite height=550 Km, lens diameter=4 m.

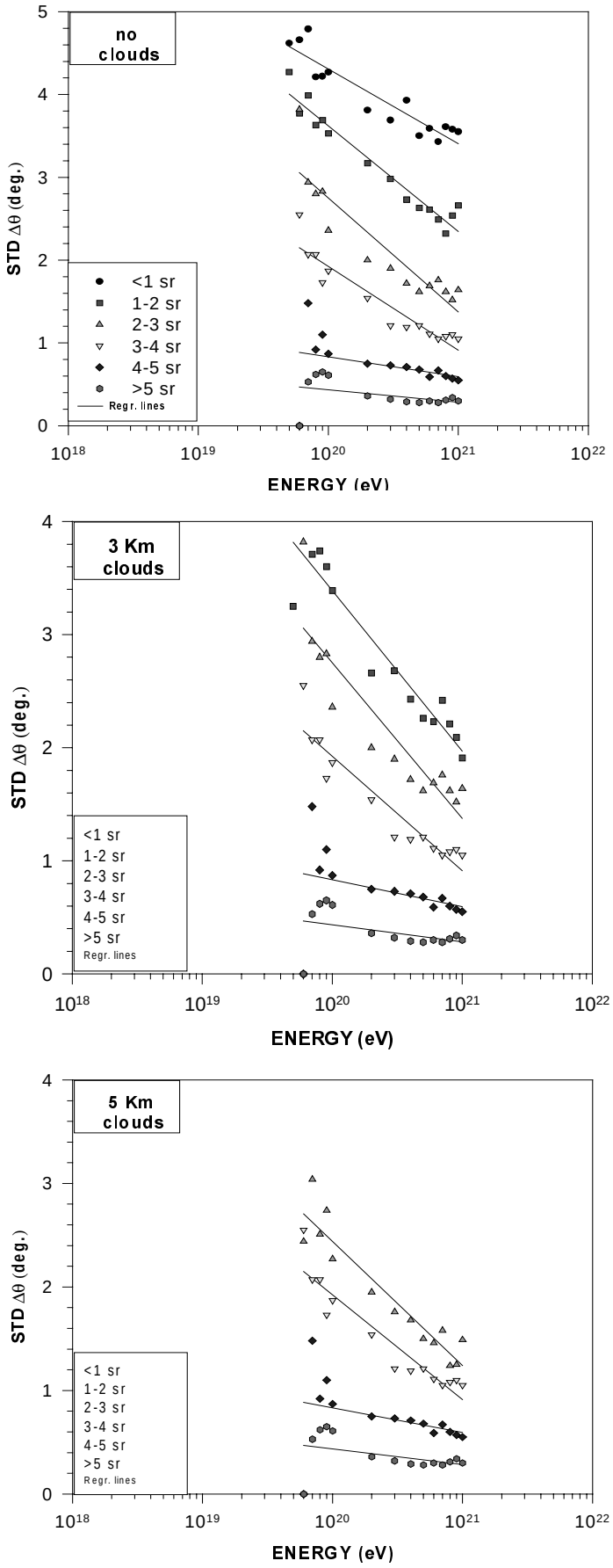

Fig. 25. Zenith angular resolution at different solid angle bins. Satellite height=550 Km, lens diameter=2 m.

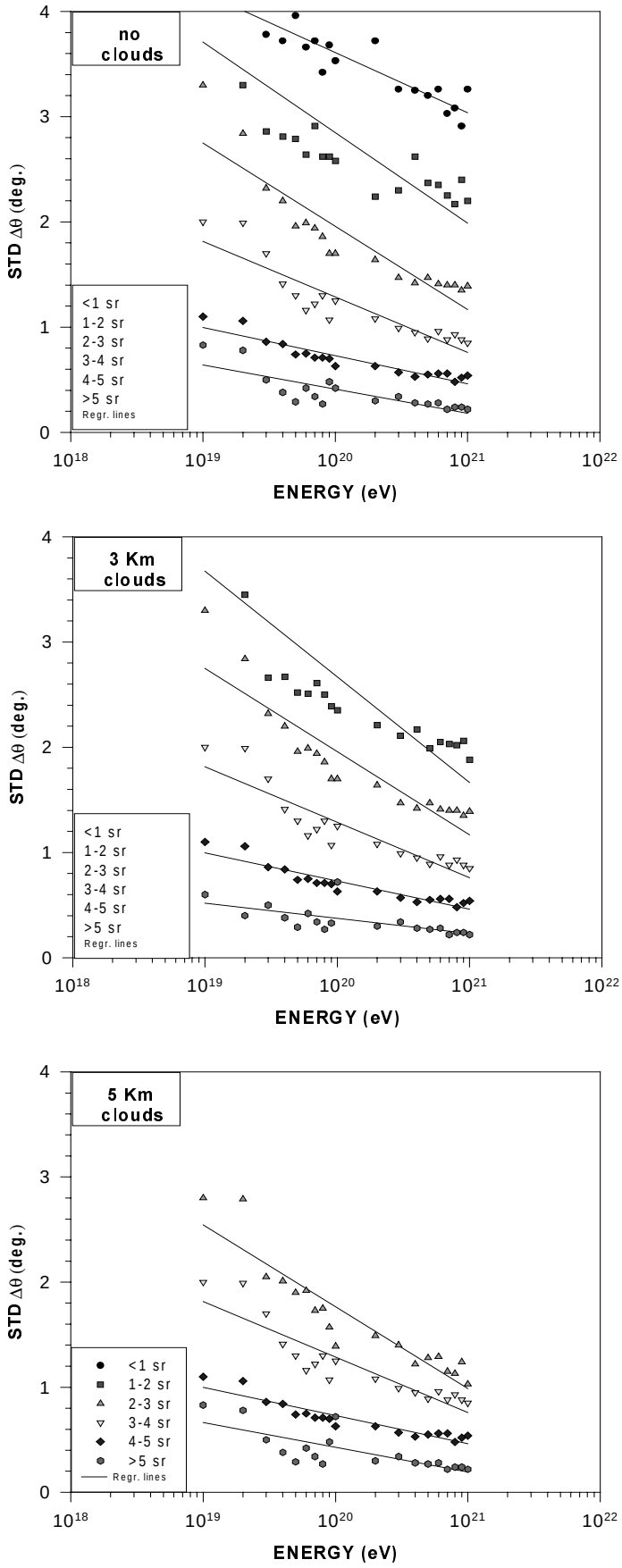

Fig. 26. Zenith angular resolution at different solid angle bins. Satellite height=400 Km, lens diameter=4 m.

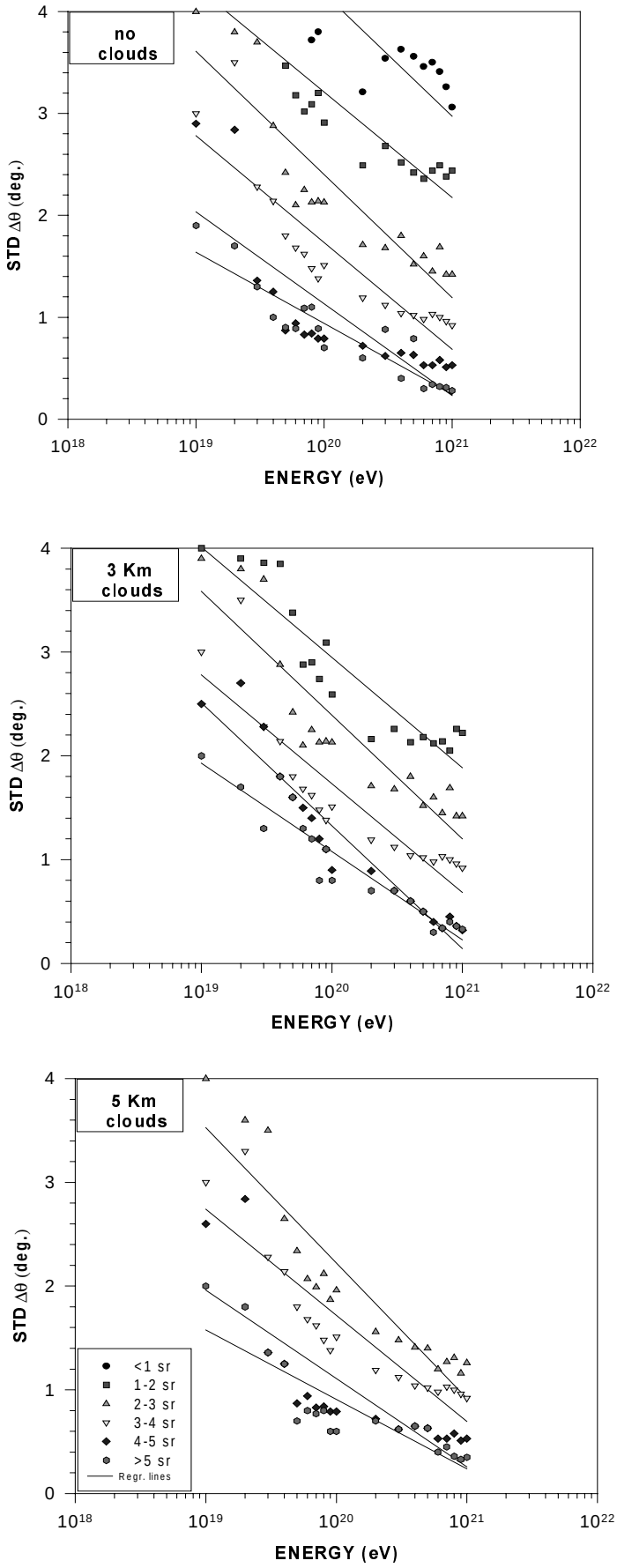

Fig. 27. Zenith angular resolution at different solid angle bins. Satellite height=400 Km, lens diameter=2 m.

4.2.3 Counting rate

Expected counting rate for the above mentioned configurations have been obtained folding the correspondent effective trigger aperture with the primary energy spectrum given by Fly's Eye [6] in the range $10^{19} - 10^{20}$ eV and extrapolated up to 10^{21} eV. A ***conservative*** duty cycle of 10% has been considered in calculating the count rate (we hope to give a better estimation of duty cycle in the near future). As previously said, also the count rates take into account only the events landing inside the FOV at the surface ground level. This choice has been preferred for accounting in the successive simulations the capability of the system in determine mass composition measurements using the Cerenkov signal reflected from clouds and sea (to be inserted in the AW simulation program).

Figure 28 shows the expected count rate curves as a function of the primary particle energy for the four simulated configurations but plotting only the "no clouds" data series. Table 2 summarizes the expected counting rate in events/year.

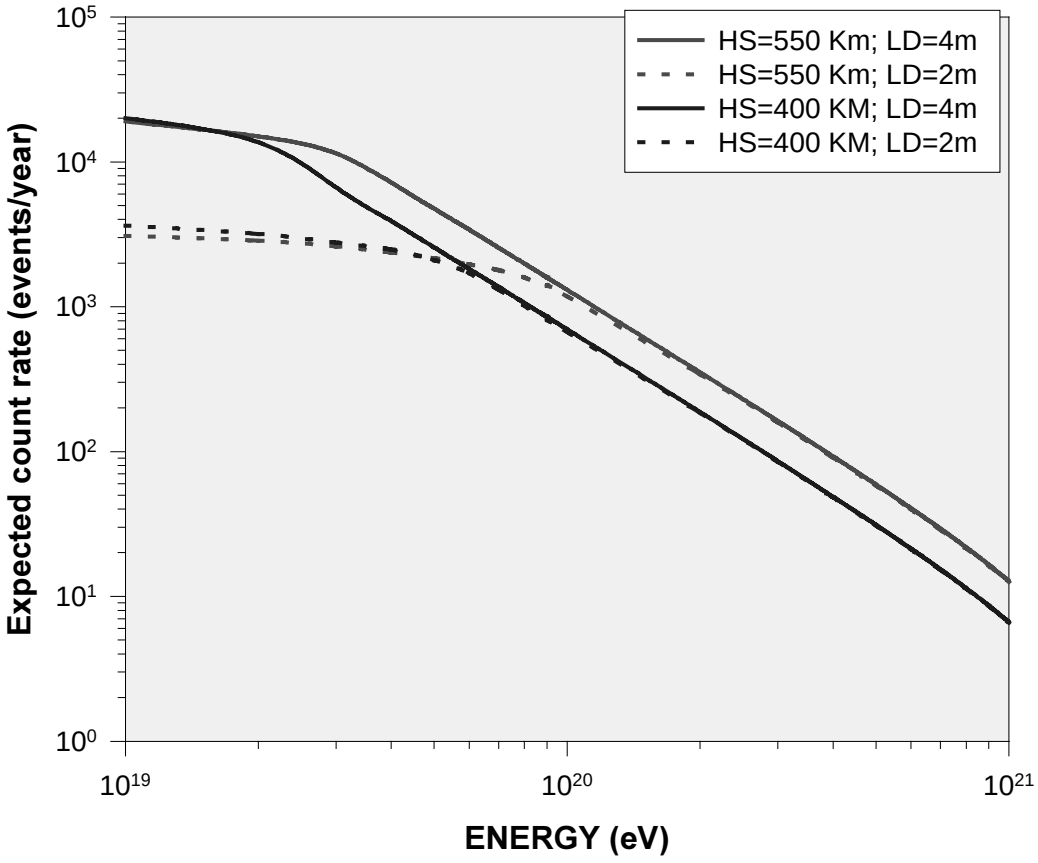

Fig. 28. Expected count rates in a year of satellite operation.

TABLE 2

Energy (eV)≥	HS=550Km;LD=4m **10% duty cycle** EVENTS/YEAR	HS=550Km;LD=2m **10% duty cycle** EVENTS/YEAR	HS=400Km;LD=4m **10% duty cycle** EVENTS/YEAR	HS=400Km;LD=2m **10% duty cycle** EVENTS/YEAR
10^{19}	**19000**	**3050**	**20000**	**3600**
$5*10^{19}$	**4750**	**2150**	**2550**	**2100**
10^{20}	**1300**	**1150**	**700**	**670**
$5*10^{20}$	**60**	**58**	**30**	**30**
10^{21}	**12**	**12**	**6**	**6**

It is evident from the results shown in table 2 that **in one "AIRWATCH" year** of data taking could be possible to collect as many events at $E>10^{20}$ eV with a factor 50 to 100 times greater than the events detected with such enormous energy in the last 40 years.

5. Neutrinos detection with AIRWATCH FROM SPACE.

"Airwatch from space" experiment, with its 10^{13} tons of target atmosphere monitored, is the ideal candidate to a possible detection of EHE (Extreme High Energy) cosmic neutrinos if any exists. Since neutrino has no charge and a negligible small magnetic moment, its electromagnetic interactions produce no directly observable effect. Its interactions are considered as being mediated exclusively by the weak interaction. The cross section is expected to be very small and increasing proportionally at √E, as shown in figure 29.

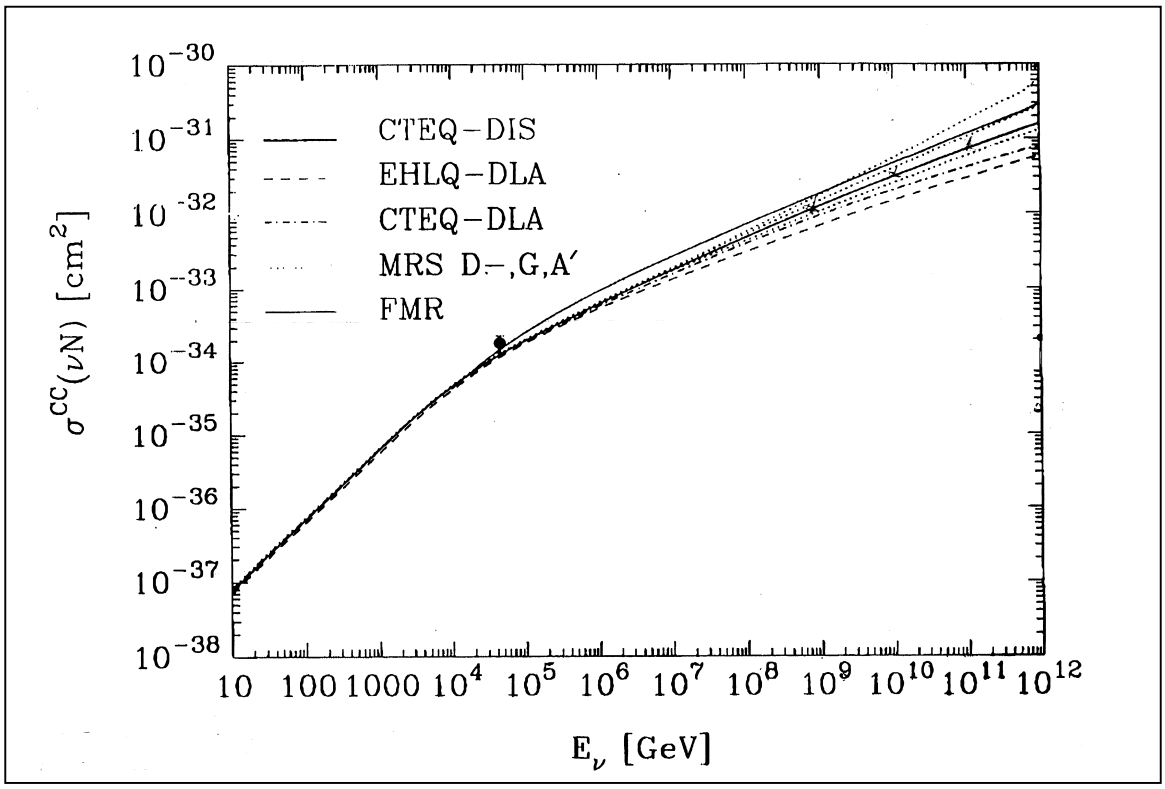

Fig. 29. Neutrino cross section.

Although the interaction is very weak, a sufficient neutrino flux could, at energy E≥ 10^{19} eV, be responsible for producing showers of secondary particles of a detectable intensity in the effective thickness of the target atmosphere.

The more accredited mechanisms of neutrinos production in the Universe are the "Top-Down" and Bottom-Up" processes. In the "Bottom-Up" scenario UHE (Ultra High Energy) particles (E≥10^{18}) are accelerated through a mechanism involving first order Fermi acceleration theory. EHE γ-rays and neutrinos are produced only in secondary processes, mainly from the decay of photoproduced pions and photodisintegration resulting from thr GZK interaction of EHE nucleons and γ-rays with the 2.7° K background photons, during propagation in the intergalactic space []. In the "Top-Down" scenario the EHE particles arise from the decay of massive (non-relativistic) "X" particles (gauge bosons, Higgs bosons,…) released in the recent cosmological epoch from collapsing and/or annihilating cosmic string,

monopoles,etc… The fundamental decay products of the X particles would be quarks and leptons that would produce hadronics jets consisting of mainly pions and a small fraction of nucleons. The pions would eventually decay into photons, neutrinos (antineutrinos) and electrons (positrons), with maximum energy, without any acceleration process.

Without entering deeply in the Top-Down and Bottom-Up scenario, we put our attention in evaluating the sensitivity of "AIRWATCH FROM SPACE" to neutrino detection. Comparison of neutrino rate expectation for planned experiment as Hi-Res and Telescope Array [7], with our derived expected rate for neutrinos (adopting the same assumptions as the experiments above mentioned) are presented.

We consider candidate neutrino events those showers that have developed deep in the atmosphere exceeding 2000 g/cm^2. Simple calculation assuming, for hadrons and gamma rays, interaction length of the order of 50-100 g/cm^2 at 10^{19} eV tell us that the probability of hadrons and gamma rays initiating EAS at deeper than 2000 g/cm^2 is less than $2*10^{-9}$. The probability of interaction of neutrinos at deeper than 2000 g/cm^2 is $\approx 2*10^{-5}$.

Figure 30 shows the geometry of the earth-satellite system. It is evident that shower directions must be greater than 70° otherwise there is not enough slant dept along the axis for the secondary shower to start deeper than 2000 g/cm^2 and develop above ground level. Moreover to separate hadrons and gamma rays event from neutrino candidates events, we have to detect events with axis falling inside the FOV to make possible the measurement of the maximum of the electromagnetic cascade of the shower. This is accomplished through the Cerenkov reflected signal on the earth surface.

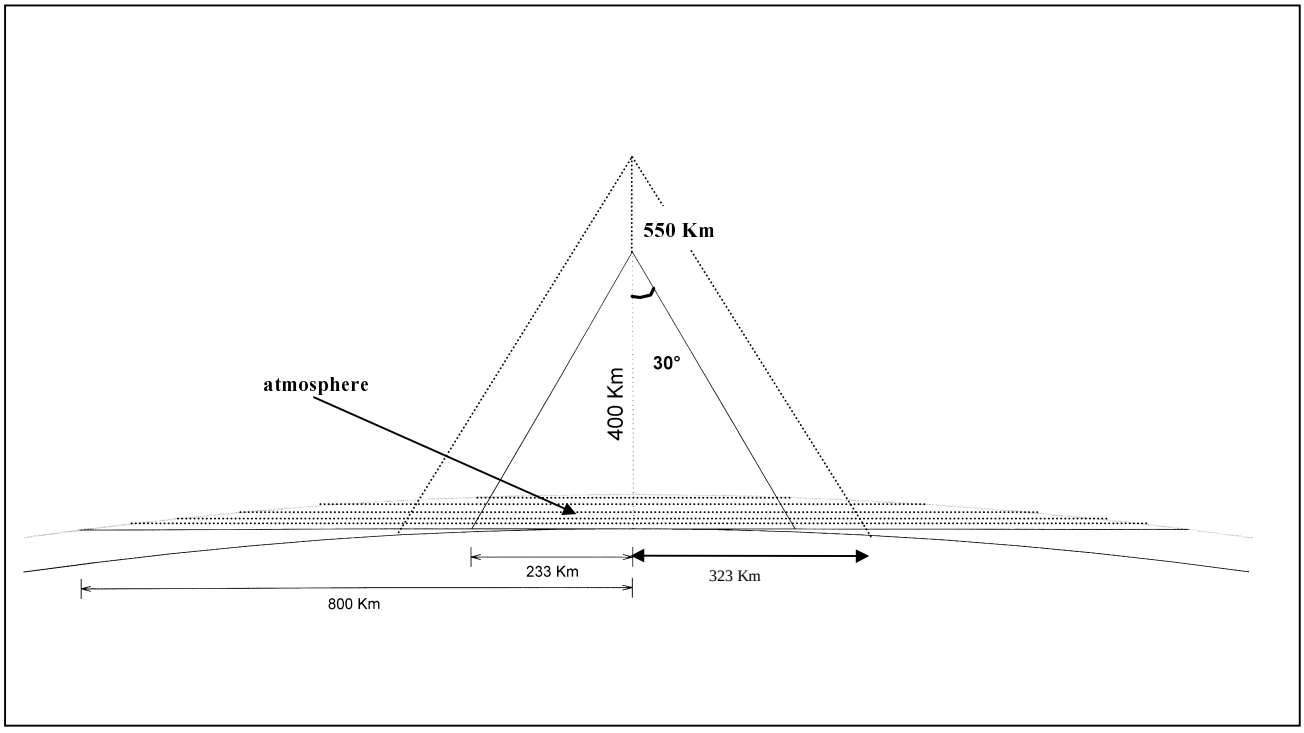

Fig. 30. Satellite-Earth system.

In figure 31 are represented the focal plane and the intercepted fiducial volume of the atmosphere by the F.O.V.. A nucleon shower has been represented with a straight line and a solid segment simulating the developing shower. A neutrino-induced shower is also represented with its developing cascade. The differences between the two showers are evident. They start developing in very different slant atmospheric dept, but at the focal plane detector their projected tracks are coincident. Then only with the reflected Cerenkov light from earth surface, represented with small dots, makes it possible to distinguish each to the other.

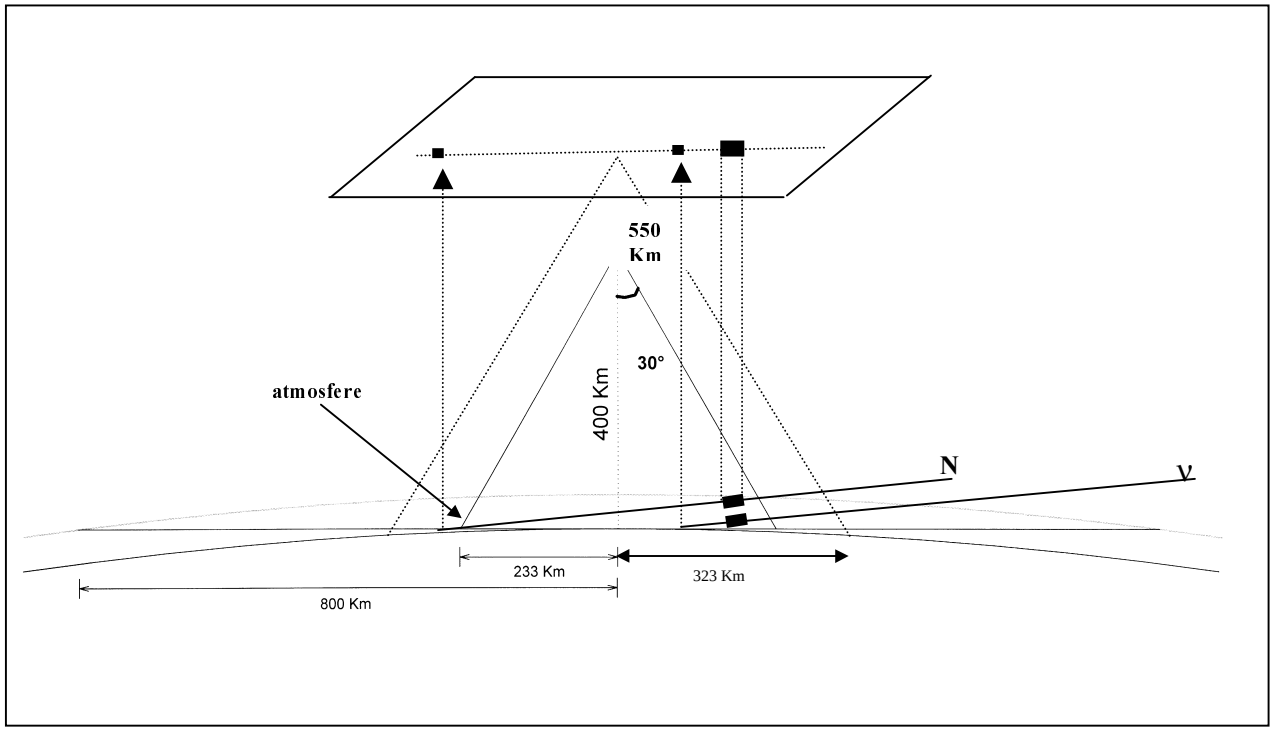

Fig. 31. Representation of a nucleon and a neutrino event.

Table 2 shows the integral ν_e flux above 10^{19} eV for different assumption of the neutrino mass in the framework of Topological Defect. The expected event rate by HiRes (HR), Telescope Array (TA) and AIRWATCH (AW) are also shown.

TABLE 3

$m_x=10^{16}$ GeV $m_\nu=0$ eV	$m_x=10^{15}$ GeV $m_\nu=1$ eV	$m_x=10^{16}$ GeV $m_\nu=0$ eV	Observed Cosmic Rays
$1.4*10^{-6}$ ($Km^{-2}*sec^{-1}*sr^{-1}$)	$4.4*10^{-7}$ ($Km^{-2}*sec^{-1}*sr^{-1}$)	$3.8*10^{-7}$ ($Km^{-2}*sec^{-1}*sr^{-1}$)	$1.4*10^{-8}$ ($Km^{-2}*sec^{-1}*sr^{-1}$)
.23 (HR), .41 (TA) Events/Yr	.08 (HR), .14 (TA) Events/Yr	.07 (HR), .12 (TA) Events/Yr	
80 (AW) Events/Yr	28 (AW) Events/Yr	24 (AW) Events/Yr	

6. Conclusions and future plans

One of the challenges of the "AIRWATCH FROM SPACE" was to demonstrate that is possible to obtain reliable information on the showers even at the primary energies of the order of 10^{19} eV. These preliminary results confirm that it is possible to have a good sensitivity starting from an energy threshold of 10^{19} eV and extending up to 10^{21} eV. Turning the energy threshold down to 10^{19} eV is very important for:

- ✓ System calibration (much higher count rate expected at these energies).
- ✓ Bridging the energy spectrum from 10^{19} to 10^{21} eV (using available data of ground base experiments at the lower energy region).
- ✓ Including the Greisen-Zatsepin-Kuzmin (GZK) cutoff region ($E \approx 5*10^{19}$)[6].
- ✓ Increasing the probability to detect possibly, EHE cosmic neutrino events.

This can be accomplished, however, only if a wide-angle optics and a fast detector are used in combination with a efficient read-out electronics.
We underline that the fundamental characteristic of a wide-angle optic (size, aperture, point spread function) and of a single photocounting detector (Q.E., intrinsic electronic noise, resolving time) must be optimized taking into account, naturally, the physical and constructive constrains. A big effort must be done, by the people involved in the project, for identifying the better solution capable to fulfil the required
performances.
Much work remains to be done to complete the simulation program. As the performance of the system is determined by all its components (optics, detector, electronics, satellite orbit ….), a continuos updating is foreseen for accounting the possible changes in one or more parameters of the project.
It is foreseen, in the near future, to insert in the AW program more detailed information for optics (filters, point spread function, segmentation…) as well as a more defined detector characteristics (resolving time, electronics noise, ….). Moreover, work is in progress for taking out the expected energy resolution as well as the expected mass composition resolution (involving Cerenkov reflected by the earth surface). We are pretty confident that such ambitious experiment is feasible and that its realization could open a new chapter in the field of the Extreme High Energy Cosmic Ray.

REFERENCES

[1] D.J. Bird et al., The Astrophysical Journal, 424: 491 (1994)
[2] G. Agnetta et al, NIM A 347, p. 521-525 (1994).
[3] D. Lamb et al., Proceedings Spie Vol. 3445, p.495-504 (1998)
[4] Il'ina et al, NIM
[5] S.C. Corbato et al. ,Nuclear Physics 28B, p. 36-39 (1992)
[6] K.Greisen, Phys. Rev. Lett. 16, 748 (1966)
[7] S. Yoshida , Proc. of Extremely High Energy Cosmic Rays: Astrophysics and Future Observatories. p 241-252 (1996)

Appendix A

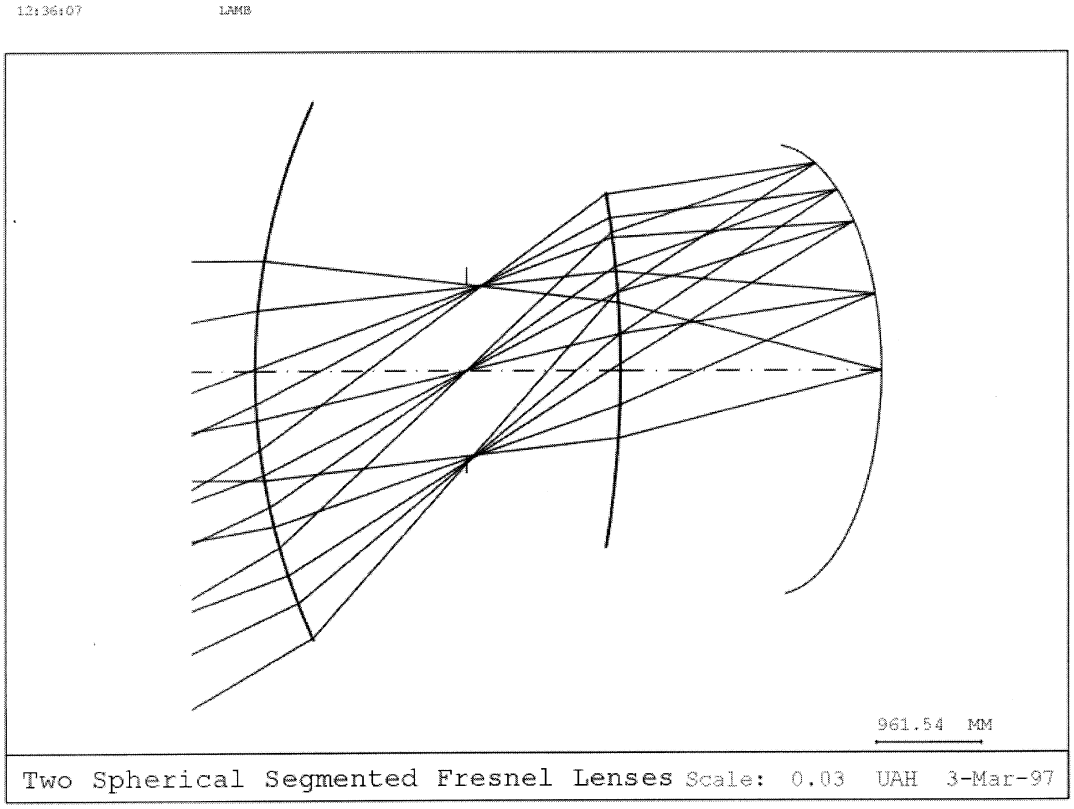
12:36:07
LAMB
961.54 MM
Two Spherical Segmented Fresnel Lenses Scale: 0.03 UAH 3-Mar-97

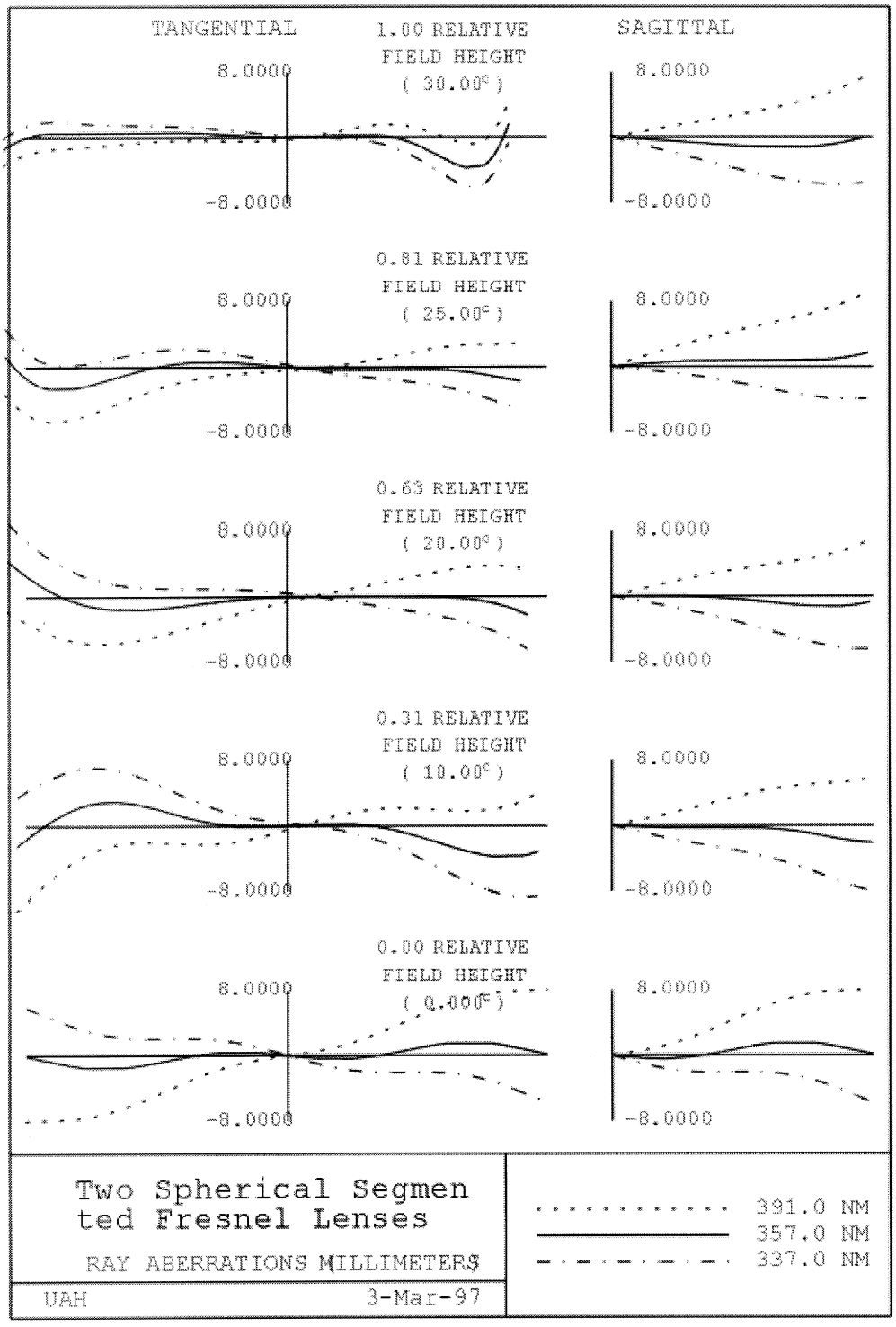
TANGENTIAL
1.00 RELATIVE
FIELD HEIGHT
(30.00°)
SAGITTAL
8.0000
-8.0000
0.81 RELATIVE
FIELD HEIGHT
(25.00°)
0.63 RELATIVE
FIELD HEIGHT
(20.00°)
0.31 RELATIVE
FIELD HEIGHT
(10.00°)
0.00 RELATIVE
FIELD HEIGHT
(0.000°)
Two Spherical Segmen
ted Fresnel Lenses
RAY ABERRATIONS MILLIMETERS
UAH
3-Mar-97
391.0 NM
357.0 NM
337.0 NM

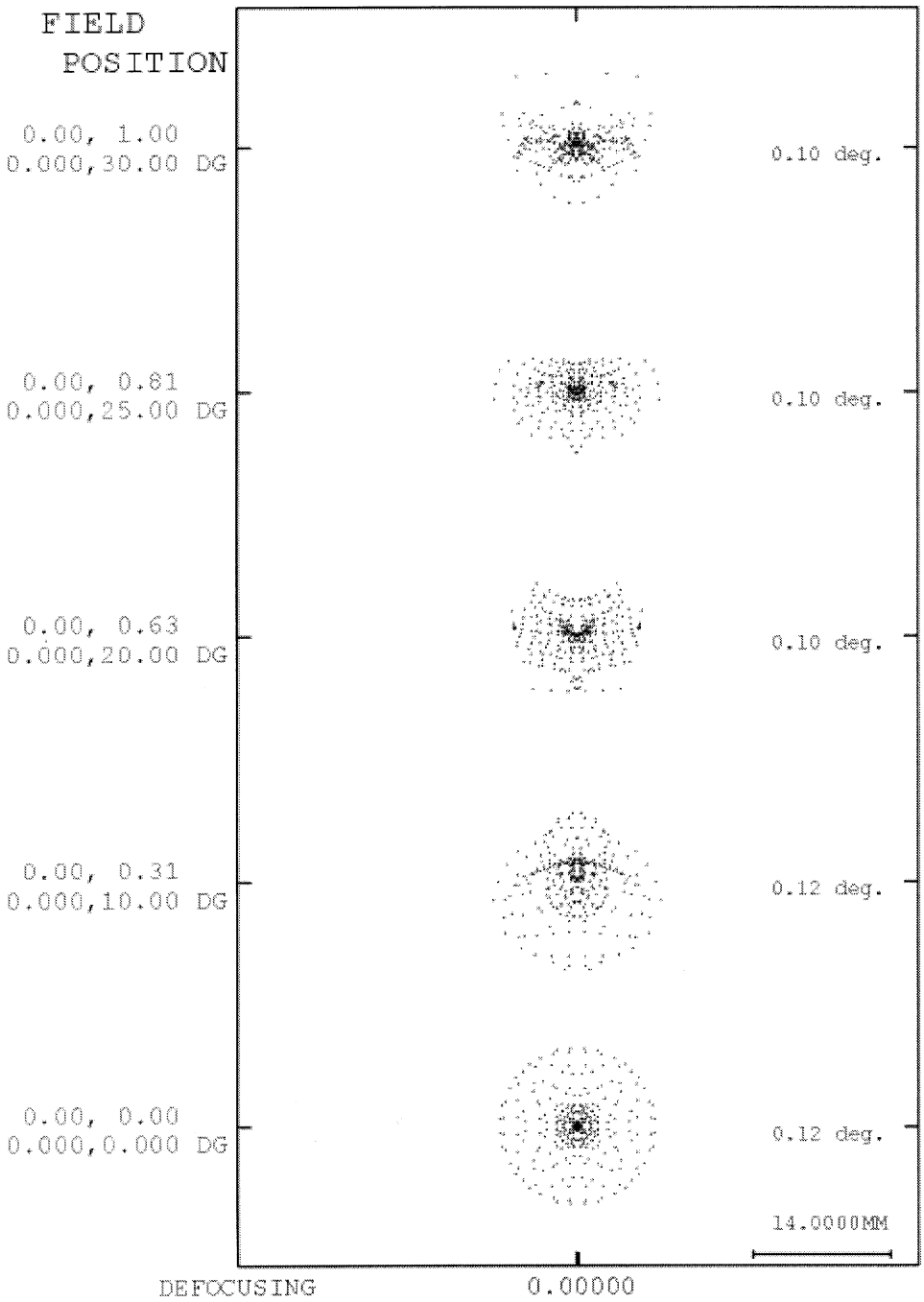

Two Spherical Segmented Fresnel Lenses

APPENDIX B

AIRWATCH UNIT and DEFINITIONS:

Background intensity ---> photons/m^2*ns*sr
wave length ---> 330 - 400 nm

Dark Sky BKG ---> 100± a factor 3 photons/m^2*ns*sr
(suggested by J. Linsley)

BKG used by OWL 330
Weekes 500 UPWARD LOOKING
Jelles 640

Meier et al. 30 - 70 DOWNWARD LOOKING
(used by TAKAHASHY)

Preliminary consideration and formulae used in the AW simulation program

Optic hypothesis:
2 double-sides Fresnel lenses whit F.O.V= ± 30° and rms spread function=.13°
(λ=337,391) (Takahashi OG. 6.1.19) (Appendix A)

DEFINITION:

PUPIL = Fresnel lens surface
PUPIL aperture = lens diameter
FOCAL PLANE = light collector
F.O.V. = total angle seen by the optic
N = N# of pixels at the Focal plane
R_p = Pupil radius
H.F.O.V. = half F.O.V. angle (degrees)
S = rms point spread angle of the optic
D_p = pixel size
Ω_{pixel} = pixel solid angle

$N=(H.F.O.V./S)^2 * \pi$ total number of pixels

$D_p=\pi*R_p^2/N$ pixel size

$\Omega_{pixel}=S*S$ pixel solid angle

Let me assume as a realistic case R_p=.75 meter, H=400 Km and F.O.V.=±30°.

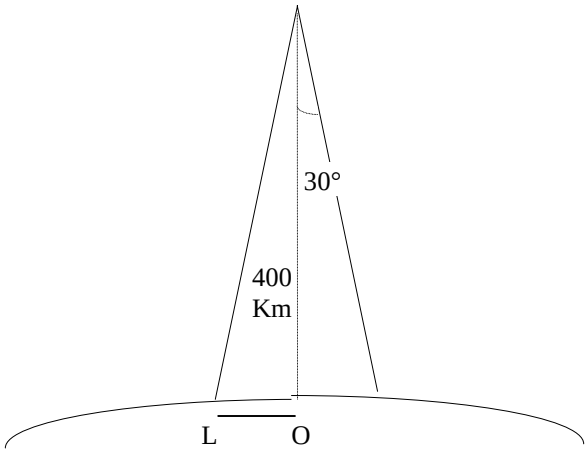

OL=400 Km*tg 30°≈231 km
target earth surface≈$167*10^3$ Km^2

N=$(30°/.13°)^2*\pi=167*10^3$ pixels
$D_p=\pi*(750)^2/163*10^3$ =10.6 mm^2

The single pixel area resolution is then = 1 Km^2

What about if I consider the earth curvature?

R=6738 Km earth radius

b=400 Km+f

$f=R-\sqrt{R^2-a^2}$

the sagitta f=4.272 Km

and the surface $(2*\pi*R*f)\approx171*10^3$ km^2

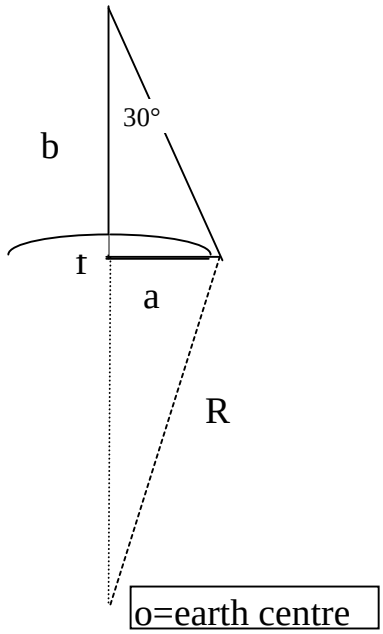

Il'ina parameterization formula

$Tm=.76*\ln(E/E_c)$
$S=2/(1+Tm/TT)$
$A=TT-Tm-2*TT*\ln(S)$
$N_e=E/1.3*\exp(A)$

Where
$TT=X/(R_l*\cos\vartheta)-1.05$
$R_l= 37.15\ g/cm^2$
$E_c=0.081\ GeV$
X=dept of atmosphere in g/cm^2
TT= dept adjusted in cascade unit
E=primary energy in GeV
S= age parameter

Kinematics of particle and measurement of zenith angle

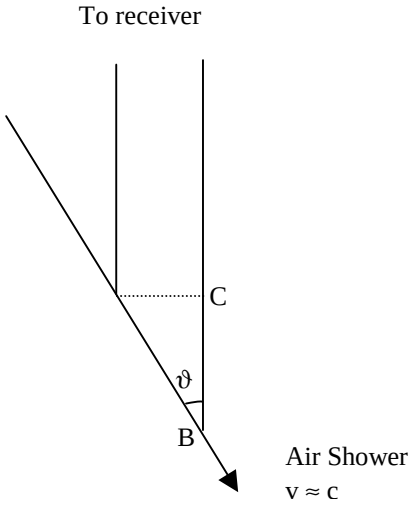

$$\Delta t = \frac{\overline{AB} + \overline{BC}}{c} = \frac{\overline{AB}}{c} \cdot (1 + \cos\vartheta) = \frac{\overline{AC}}{c \cdot \sin\vartheta} \cdot (1 + \cos\vartheta)$$

$$\frac{\sin\vartheta}{1 + \cos\vartheta} = \frac{\overline{AC}}{c \cdot \Delta t}$$

$$\vartheta = 2 \cdot \tan^{-1} \frac{\overline{AC}}{c \cdot \Delta t}$$

APPENDIX C

Standard Atmosphere

The air is assumed to be dry, and at altitudes below 86 Km the atmosphere is assumed to be homogeneously mixed with a relative volume composition leading to a constant mean molecular weight $M_0=\Sigma (n_i*M_i)/\Sigma n_i$ where n_i and M_i are the number density and molecular weight, respectively, of the ith gas species. M_0 = 28.9644 kg/Kmol. The air is treated as if it were a perfect gas, and total pressure P, temperature T, and total density ρ at any point in the atmosphere are related by the equation of state, that is, the perfect gas law, one form of which is :

$$P=\rho * R * T/M_0$$

Where R is the universal gas costant.

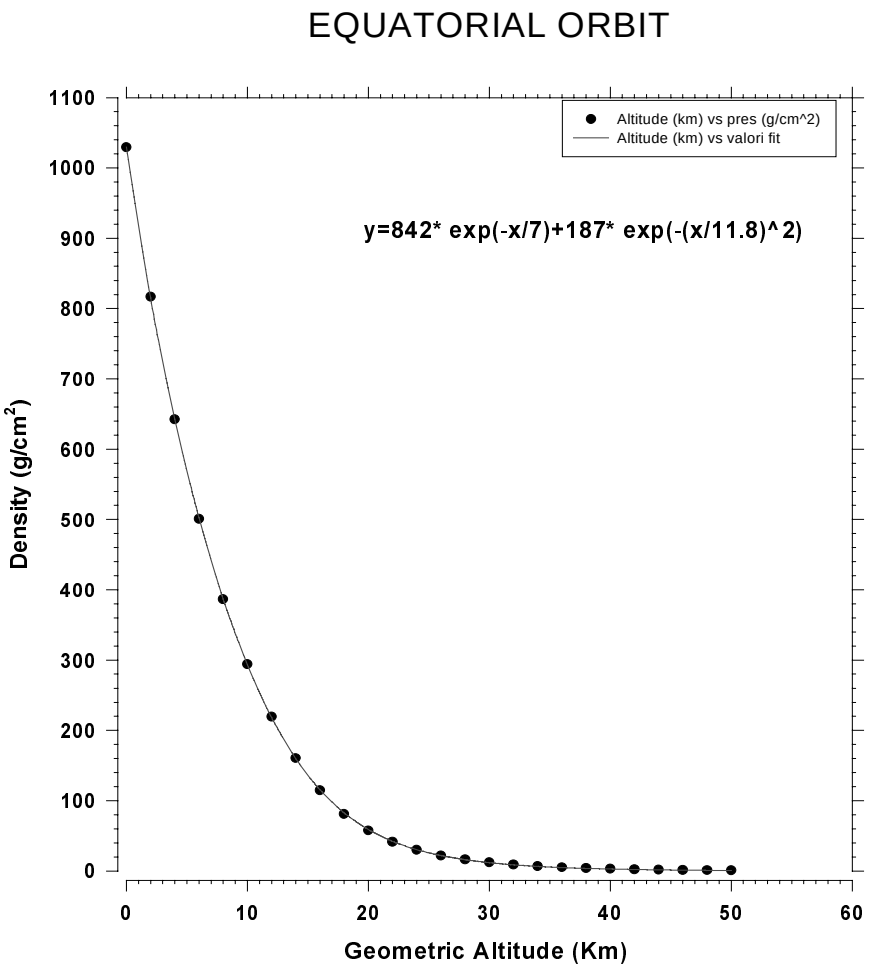

Pressure vs. temperature (equatorial latitude)

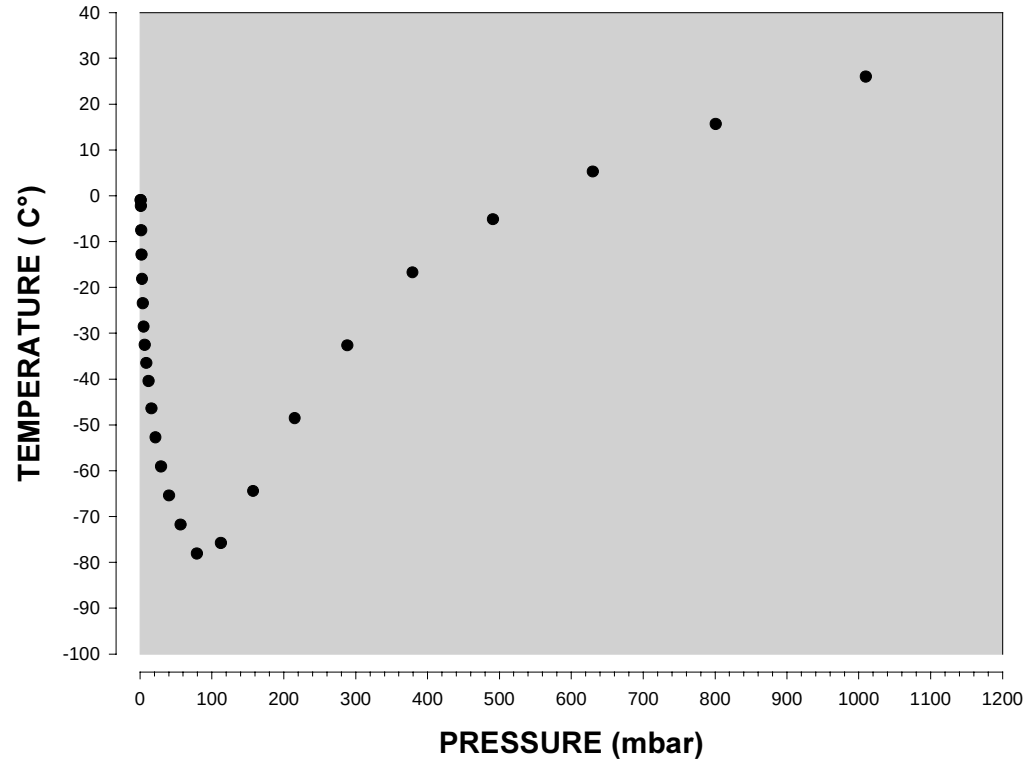

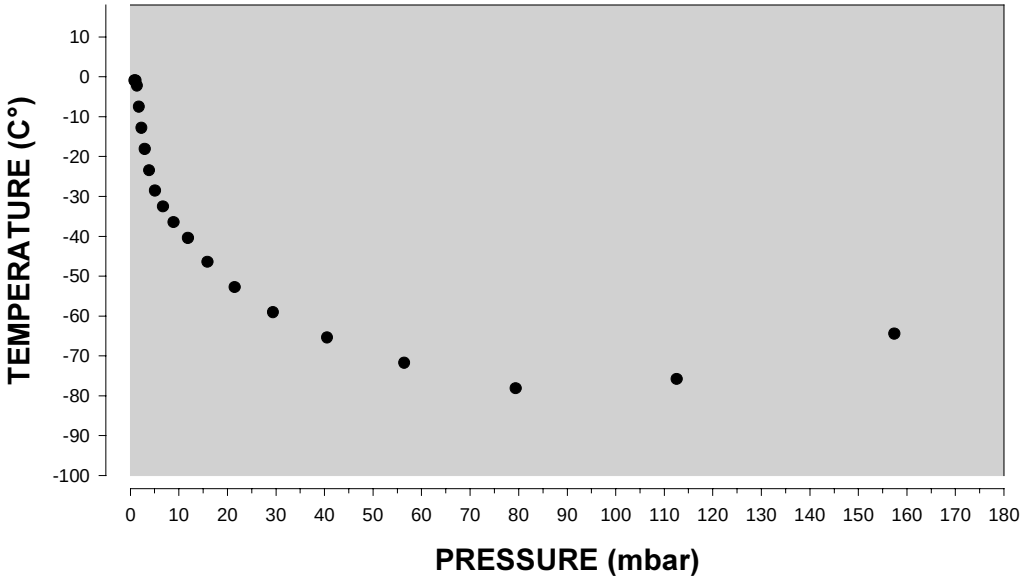

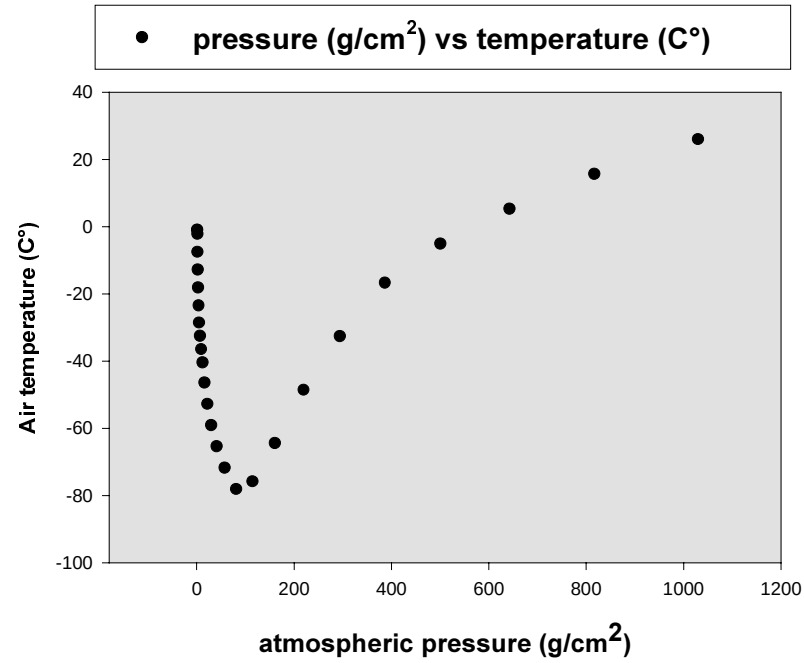
pressure (g/cm2) vs temperature (C°)
Air temperature (C°)
40
20
0
-20
-40
-60
-80
-100
0
200
400
600
800
1000
1200
atmospheric pressure (g/cm2)

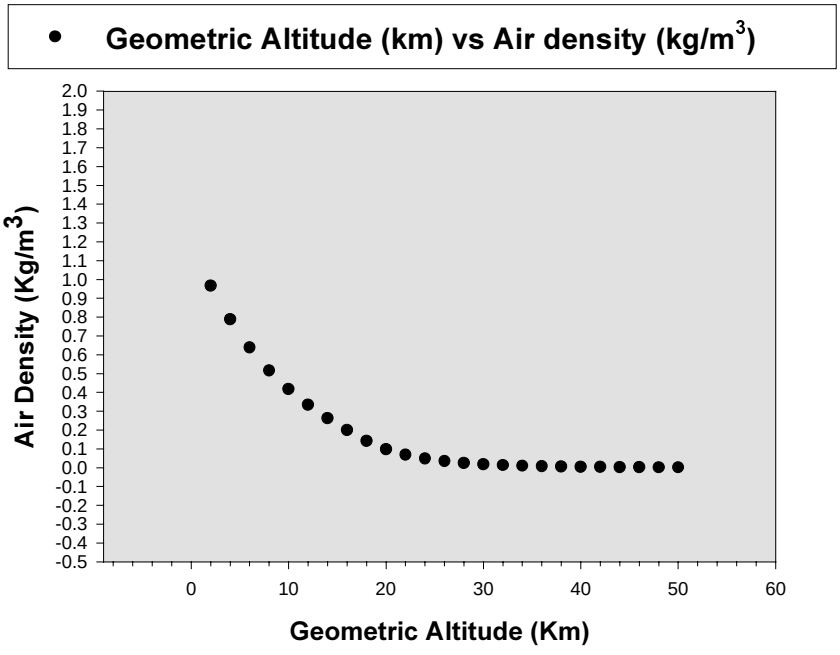
Geometric Altitude (km) vs Air density (kg/m3)
Air Density (Kg/m3)
2.0
1.9
1.8
1.7
1.6
1.5
1.4
1.3
1.2
1.1
1.0
0.9
0.8
0.7
0.6
0.5
0.4
0.3
0.2
0.1
0.0
-0.1
-0.2
-0.3
-0.4
-0.5
0
10
20
30
40
50
60
Geometric Altitude (Km)

APPENDIX D

OZONE TRANSMISSION

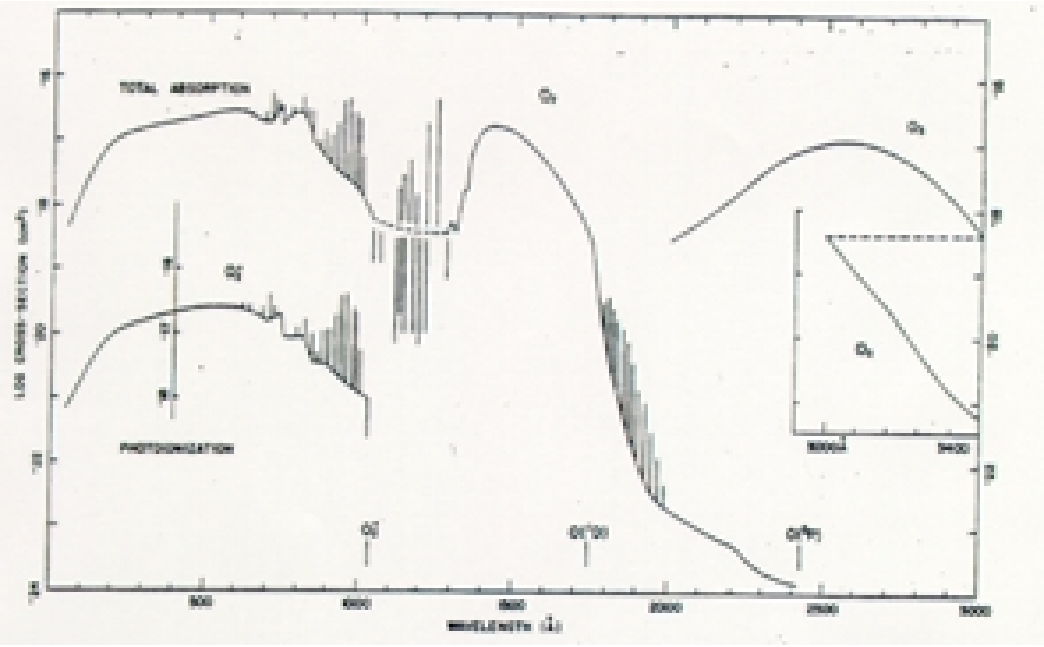

In the earth atmosphere the UltraViolet radiation (UV) is absorbed by photoelectric effect from the molecules present in air.
The UV photons produced in air from the decayment of the nitrogen molecule (N_2), which range is from 300 to 400 nm, are partially absorbed by the ozone molecule (O_3).
The transmission through the ozone layer is given by $\exp(-\sigma N)$, where σ is the total absorption cross section in cm^2 and N is the column density in cm^{-2}.
From the above figure we estimate at 331 nm, the first component of the nitrogen molecular deexcitation, an ozone molecular absorption cross section of about $5 \cdot 10^{-20}$ cm^2.
Taking into account the vertical profile of the ozone concentration (that is reported in the next figure) we found a transmission value through the ozone layer of about 75%.

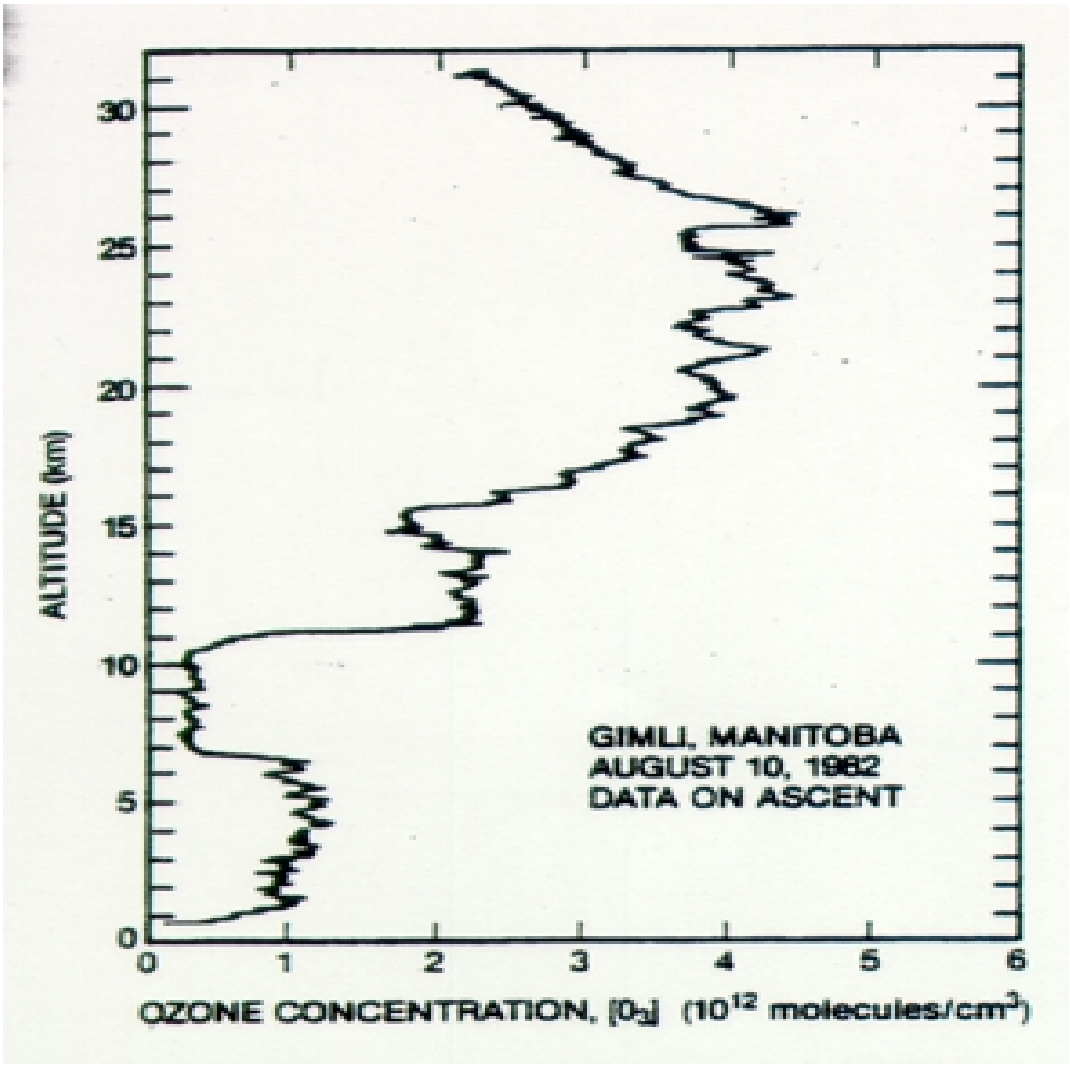
ALTITUDE (km)
0
5
10
15
20
25
30
0
1
2
3
4
5
6
GIMLI, MANITOBA
AUGUST 10, 1962
DATA ON ASCENT
OZONE CONCENTRATION, [O3] (10^12 molecules/cm^3)

APPENDIX E

Event with more than one macrocell hit.

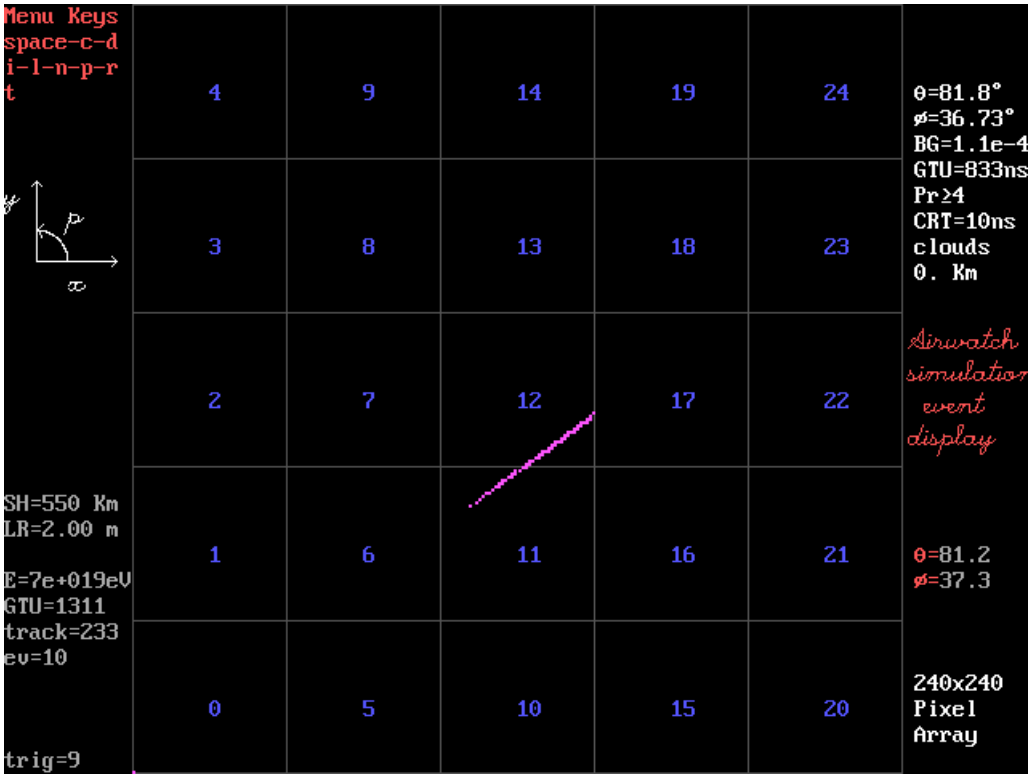

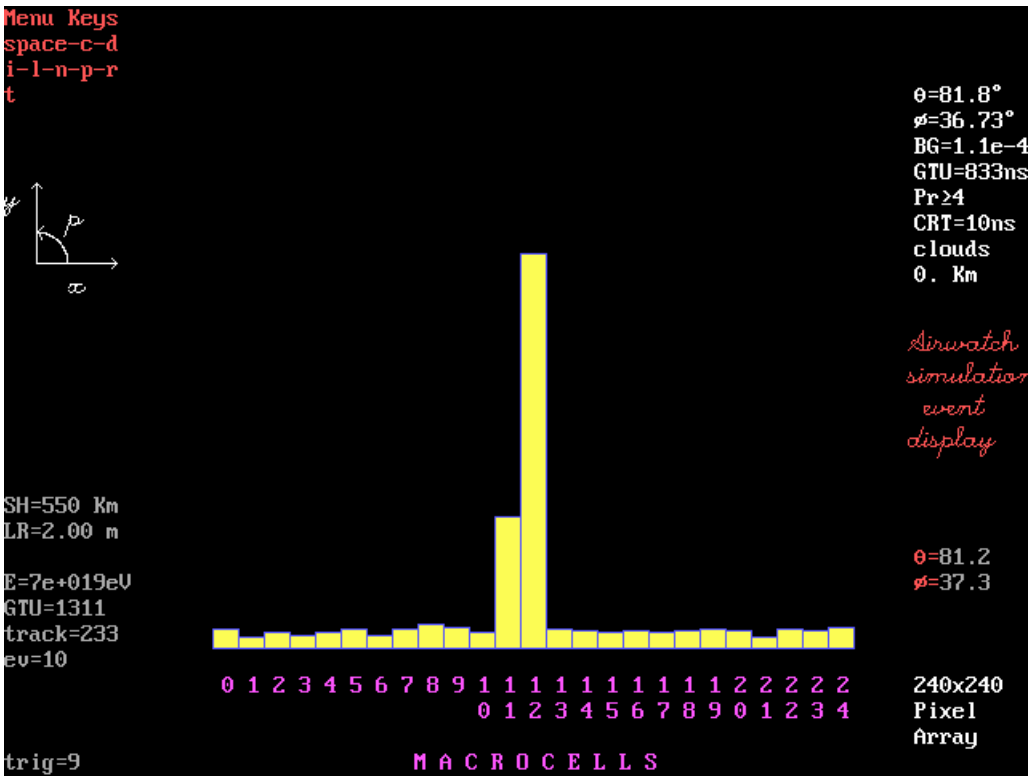

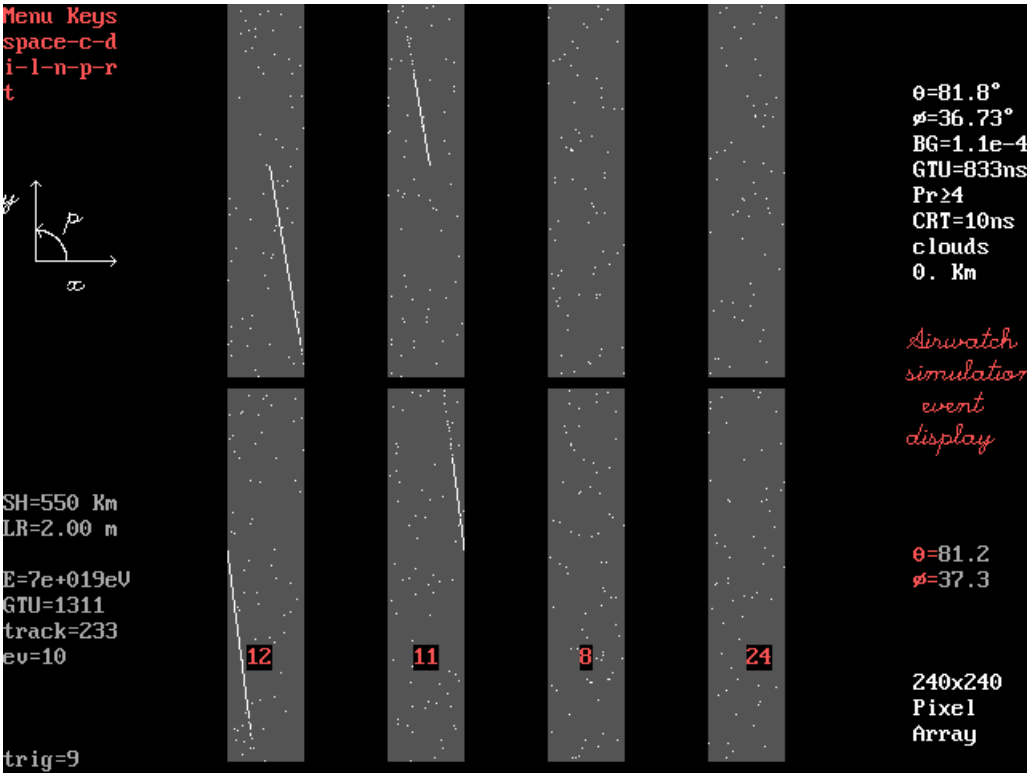
Menu Keys
space-c-d
i-l-n-p-r
t
θ=81.8°
ø=36.73°
BG=1.1e-4
GTU=833ns
Pr≥4
CRT=10ns
clouds
0. Km
Airwatch
simulator
event
display
SH=550 Km
LR=2.00 m
E=7e+019eV
GTU=1311
track=233
ev=10
12
11
8
24
θ=81.2
ø=37.3
240x240
Pixel
Array
trig=9

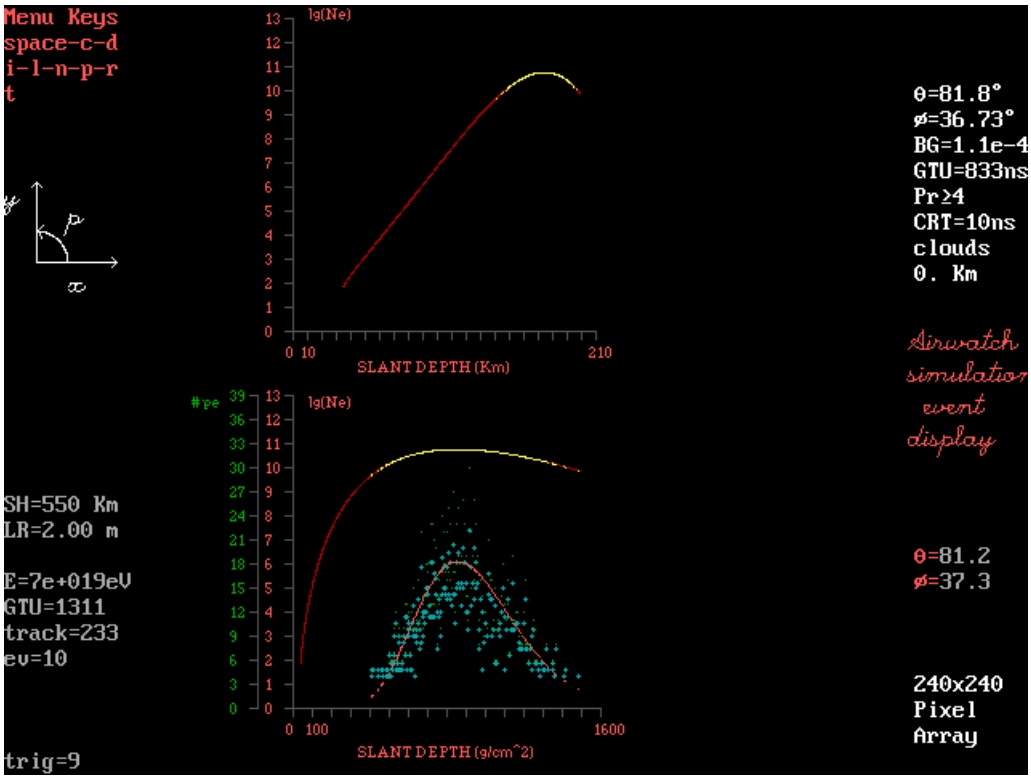
Menu Keys
space-c-d
i-l-n-p-r
t
lg(Ne)
SLANT DEPTH (Km)
#pe
lg(Ne)
SLANT DEPTH (g/cm^2)
θ=81.8°
ø=36.73°
BG=1.1e-4
GTU=833ns
Pr≥4
CRT=10ns
clouds
0. Km
Airwatch
simulator
event
display
SH=550 Km
LR=2.00 m
E=7e+019eV
GTU=1311
track=233
ev=10
θ=81.2
ø=37.3
240x240
Pixel
Array
trig=9

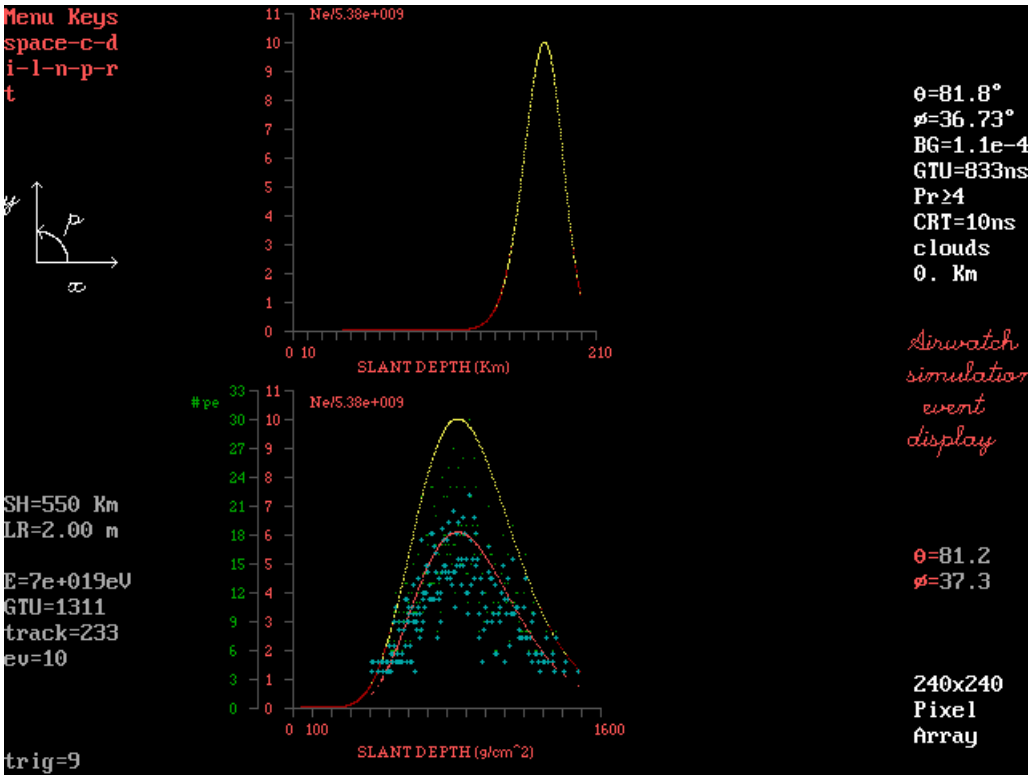
Menu Keys
space-c-d
i-l-n-p-r
t
Ne/5.38e+009
SLANT DEPTH (Km)
θ=81.8°
ø=36.73°
BG=1.1e-4
GTU=833ns
Pr≥4
CRT=10ns
clouds
0. Km
Airwatch
simulator
event
display
pe
Ne/5.38e+009
SLANT DEPTH (g/cm^2)
SH=550 Km
LR=2.00 m
E=7e+019eV
GTU=1311
track=233
ev=10
θ=81.2
ø=37.3
240x240
Pixel
Array
trig=9

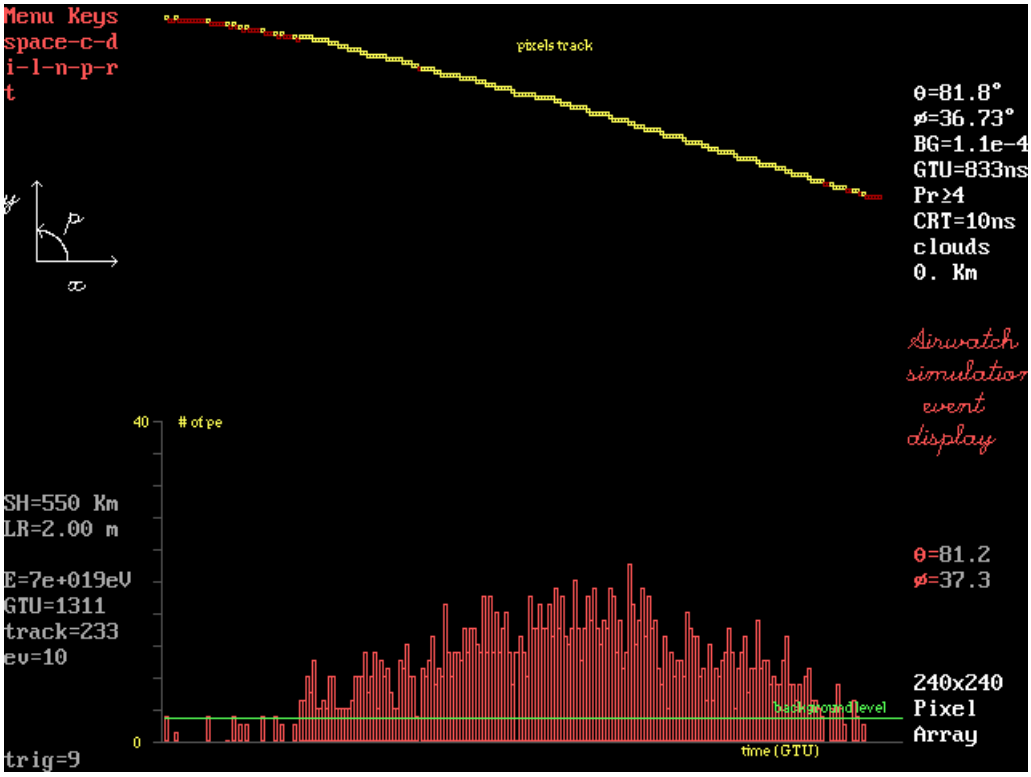
Menu Keys
space-c-d
i-l-n-p-r
t
pixels track
θ=81.8°
ø=36.73°
BG=1.1e-4
GTU=833ns
Pr≥4
CRT=10ns
clouds
0. Km
Airwatch
simulator
event
display
# of pe
background level
time (GTU)
SH=550 Km
LR=2.00 m
E=7e+019eV
GTU=1311
track=233
ev=10
θ=81.2
ø=37.3
240x240
Pixel
Array
trig=9

3 Km clouds.


Menu Keys
space-c-d
i-l-n-p-r
t
4
9
14
19
24
3
8
13
18
23
2
7
12
17
22
1
6
11
16
21
0
5
10
15
20
θ=36.17°
ø=36.66°
BG=1.1e-4
GTU=833ns
Pr≥4
CRT=10ns
clouds
3. Km
Airwatch
simulator
event
display
SH=550 Km
LR=2.00 m
E=7e+019eV
GTU=233
track=41
ev=6
θ=25.2
ø=26.6
240x240
Pixel
Array
trig=6

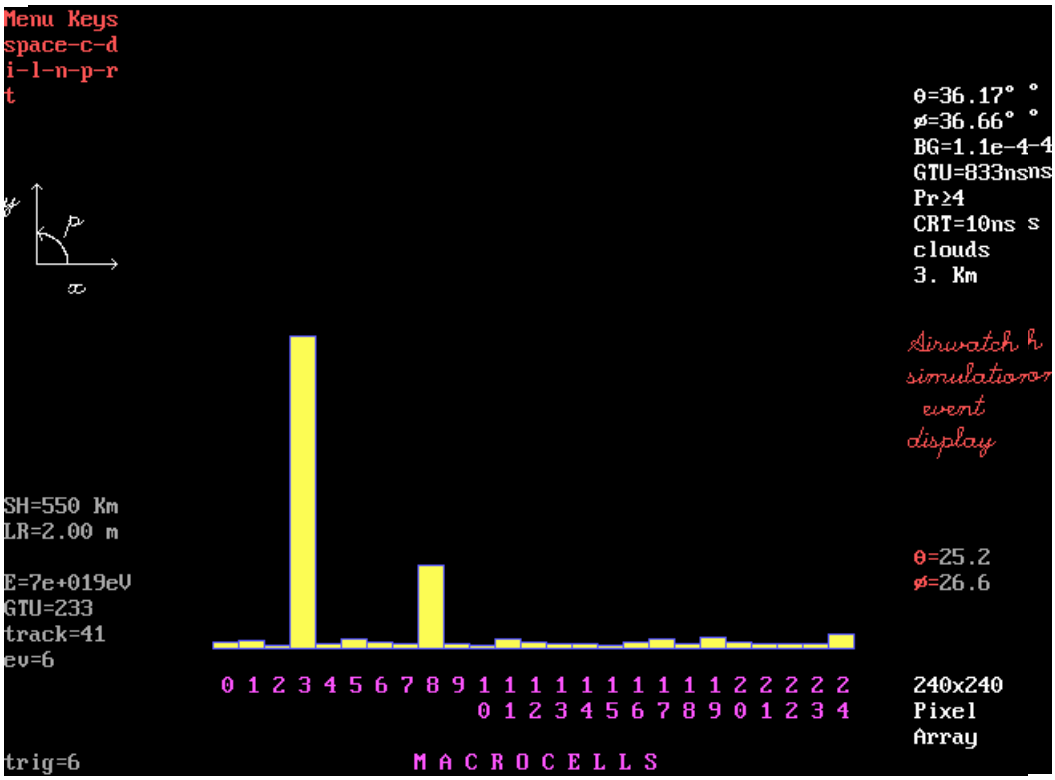
Menu Keys
space-c-d
i-l-n-p-r
t
θ=36.17° °
ø=36.66° °
BG=1.1e-4-4
GTU=833nsns
Pr≥4
CRT=10ns s
clouds
3. Km
Airwatch k
simulatoror
event
display
SH=550 Km
LR=2.00 m
E=7e+019eV
GTU=233
track=41
ev=6
θ=25.2
ø=26.6
0 1 2 3 4 5 6 7 8 9 1 1 1 1 1 1 1 1 1 2 2 2 2 2
0 1 2 3 4 5 6 7 8 9 0 1 2 3 4
240x240
Pixel
Array
trig=6
MACROCELLS

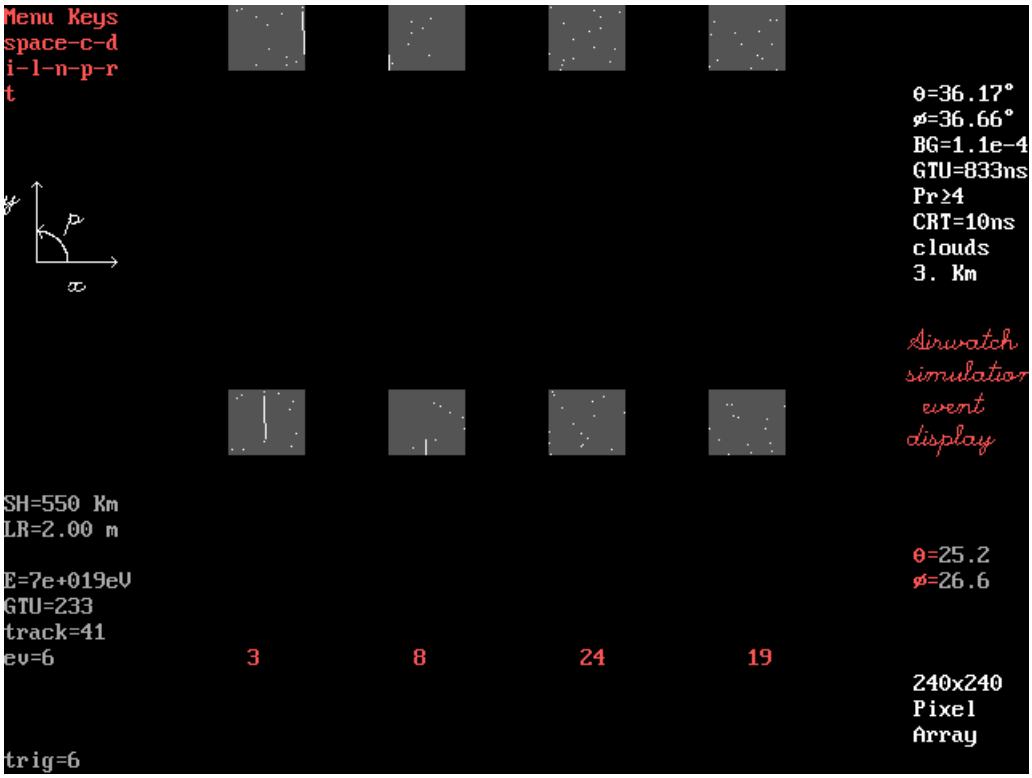
Menu Keys
space-c-d
i-l-n-p-r
t
θ=36.17°
ø=36.66°
BG=1.1e-4
GTU=833ns
Pr≥4
CRT=10ns
clouds
3. Km
Airwatch
simulation
event
display
SH=550 Km
LR=2.00 m
E=7e+019eV
GTU=233
track=41
ev=6
3
8
24
19
θ=25.2
ø=26.6
240x240
Pixel
Array
trig=6

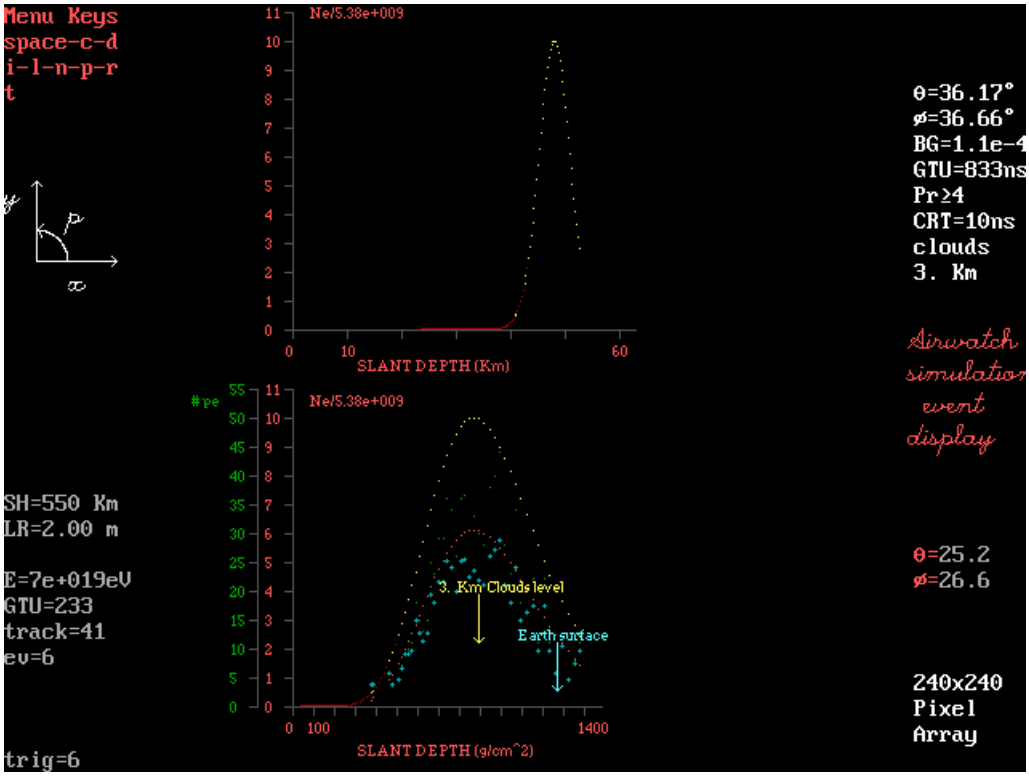
Menu Keys
space-c-d
i-l-n-p-r
t
Ne/5.38e+009
SLANT DEPTH (Km)
#pe
Ne/5.38e+009
3. Km Clouds level
Earth surface
SLANT DEPTH (g/cm^2)
θ=36.17°
ø=36.66°
BG=1.1e-4
GTU=833ns
Pr≥4
CRT=10ns
clouds
3. Km
Airwatch
simulation
event
display
SH=550 Km
LR=2.00 m
E=7e+019eV
GTU=233
track=41
ev=6
θ=25.2
ø=26.6
240x240
Pixel
Array
trig=6

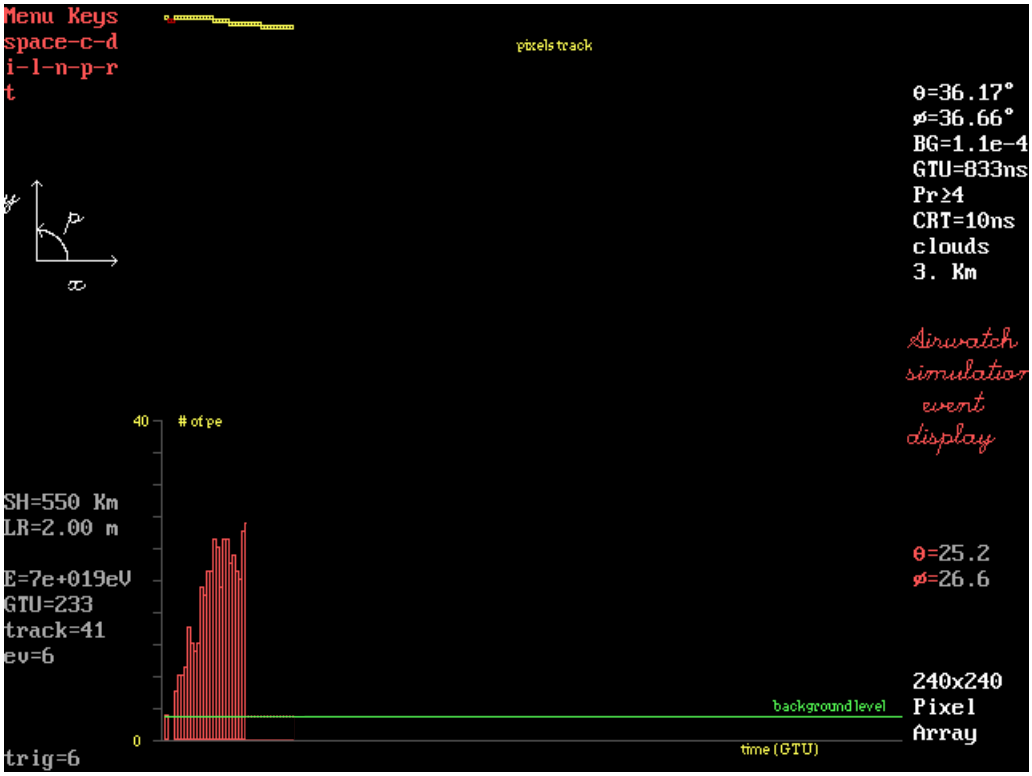
Menu Keys
space-c-d
i-l-n-p-r
t
pixels track
θ=36.17°
ø=36.66°
BG=1.1e-4
GTU=833ns
Pr≥4
CRT=10ns
clouds
3. Km
Airwatch
simulator
event
display
40
# of pe
SH=550 Km
LR=2.00 m
E=7e+019eV
GTU=233
track=41
ev=6
θ=25.2
ø=26.6
240x240
Pixel
Array
background level
0
time (GTU)
trig=6

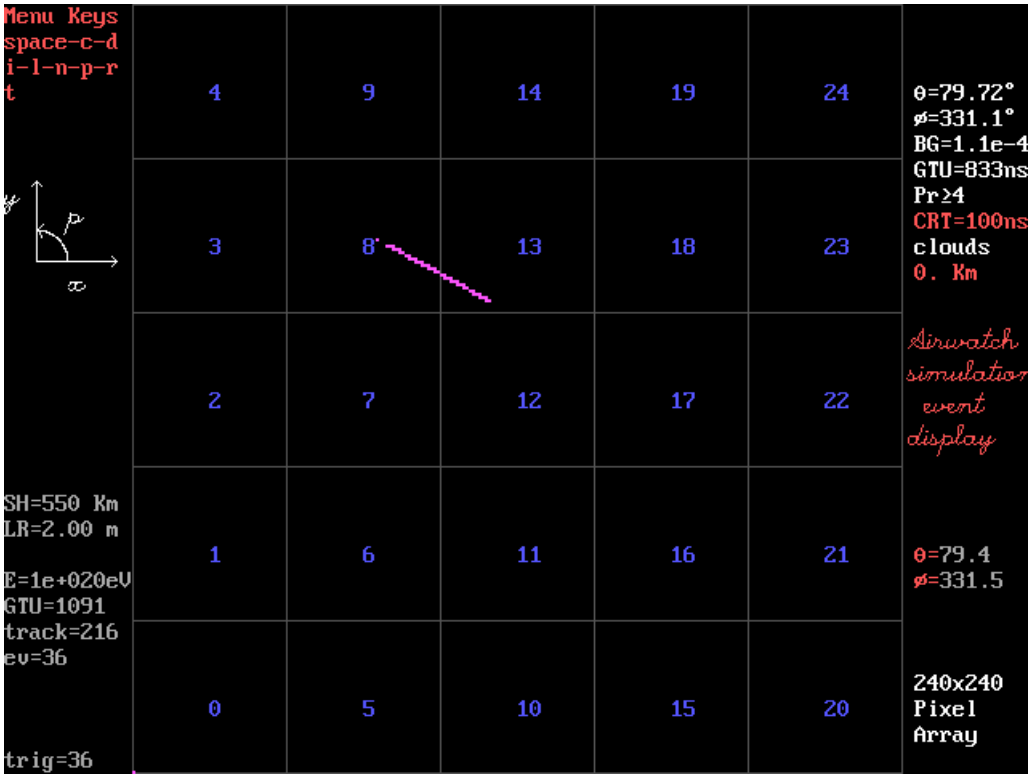
Menu Keys
space-c-d
i-l-n-p-r
t
4
9
14
19
24
3
8
13
18
23
2
7
12
17
22
1
6
11
16
21
0
5
10
15
20
θ=79.72°
ø=331.1°
BG=1.1e-4
GTU=833ns
Pr≥4
CRT=100ns
clouds
0. Km
Airwatch
simulation
event
display
SH=550 Km
LR=2.00 m
E=1e+020eV
GTU=1091
track=216
ev=36
trig=36
θ=79.4
ø=331.5
240x240
Pixel
Array

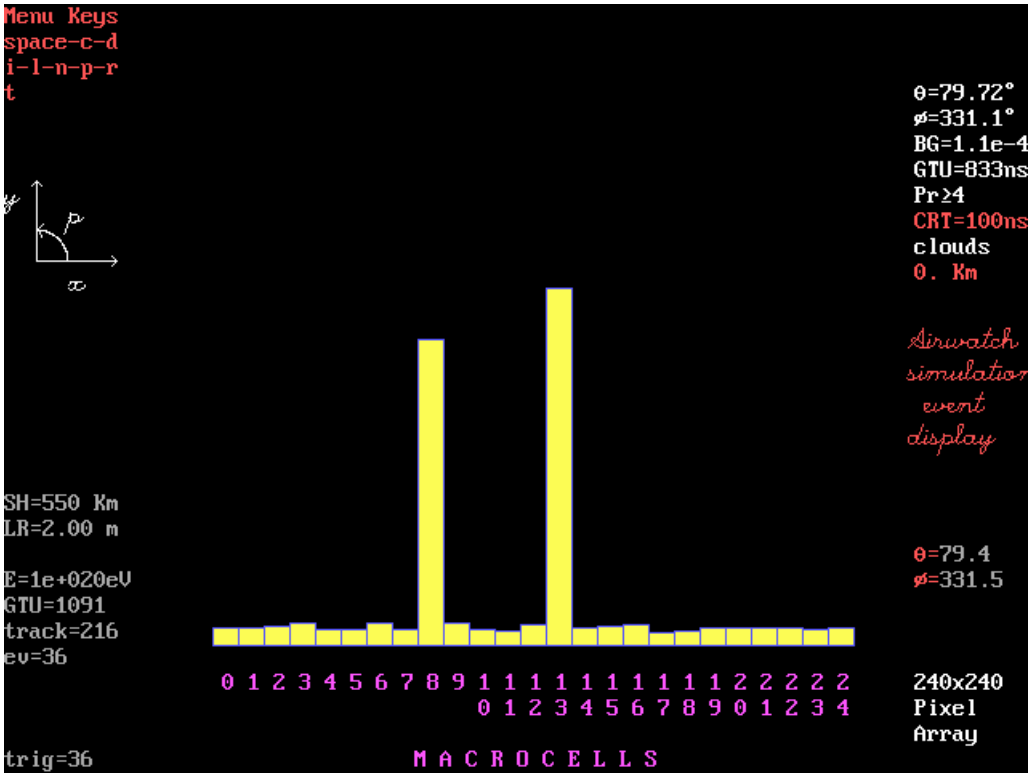
Menu Keys
space-c-d
i-l-n-p-r
t
θ=79.72°
ø=331.1°
BG=1.1e-4
GTU=833ns
Pr≥4
CRT=100ns
clouds
0. Km
Airwatch
simulation
event
display
SH=550 Km
LR=2.00 m
E=1e+020eV
GTU=1091
track=216
ev=36
θ=79.4
ø=331.5
0 1 2 3 4 5 6 7 8 9 1 1 1 1 1 1 1 1 1 2 2 2 2 2
0 1 2 3 4 5 6 7 8 9 0 1 2 3 4
240x240
Pixel
Array
trig=36
MACROCELLS

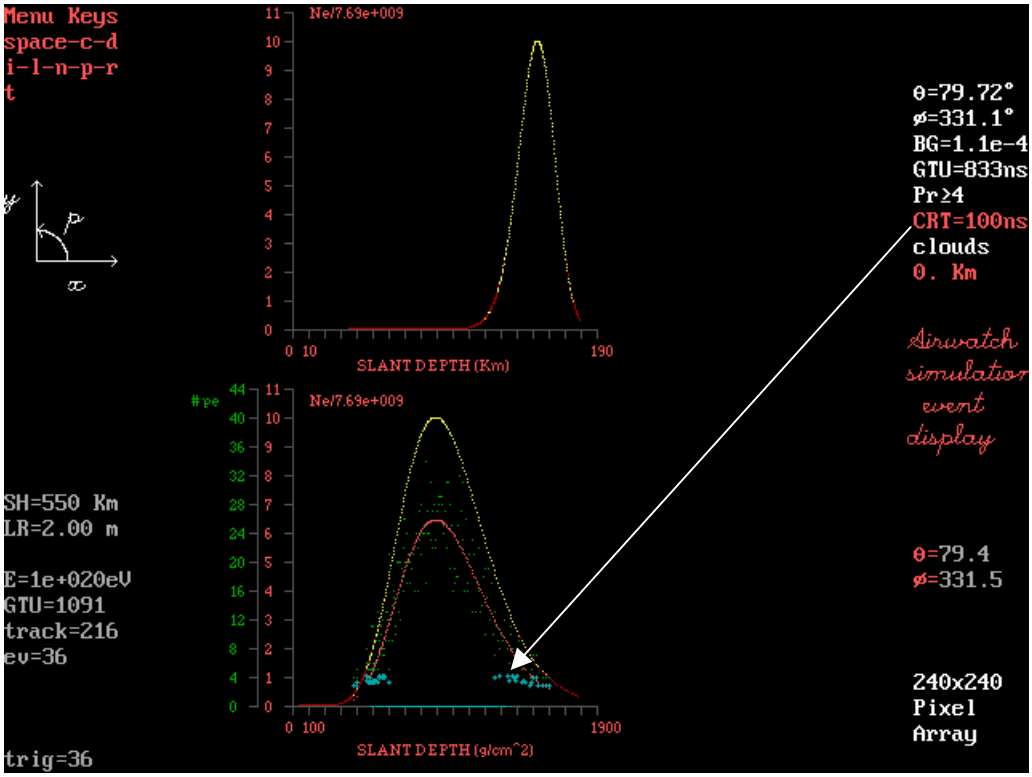
Menu Keys
space-c-d
i-l-n-p-r
t
Ne/7.69e+009
SLANT DEPTH (Km)
θ=79.72°
ø=331.1°
BG=1.1e-4
GTU=833ns
Pr≥4
CRT=100ns
clouds
0. Km
Airwatch
simulator
event
display
#pe
Ne/7.69e+009
SLANT DEPTH (g/cm^2)
SH=550 Km
LR=2.00 m
E=1e+020eV
GTU=1091
track=216
ev=36
θ=79.4
ø=331.5
240x240
Pixel
Array
trig=36

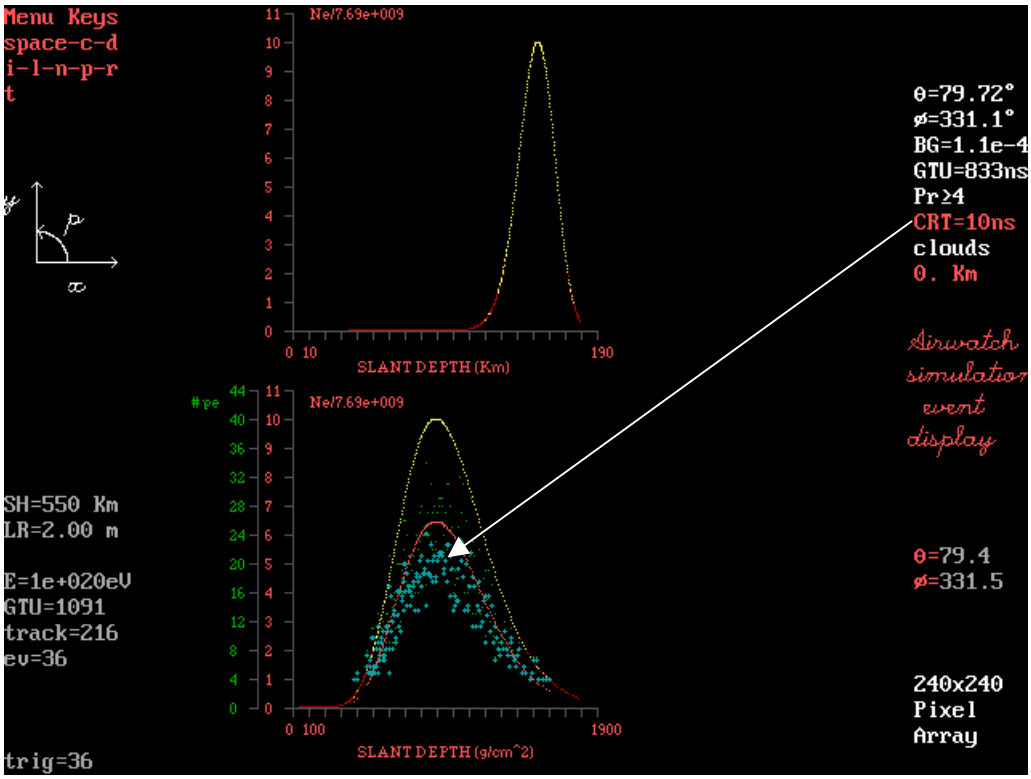
Menu Keys
space-c-d
i-l-n-p-r
t
Ne/7.69e+009
SLANT DEPTH (Km)
θ=79.72°
ø=331.1°
BG=1.1e-4
GTU=833ns
Pr≥4
CRT=10ns
clouds
0. Km
Airwatch
simulator
event
display
#pe
Ne/7.69e+009
SLANT DEPTH (g/cm^2)
SH=550 Km
LR=2.00 m
E=1e+020eV
GTU=1091
track=216
ev=36
θ=79.4
ø=331.5
240x240
Pixel
Array
trig=36